RSC Advances

PAPER

View Article Online
View Journal | View Issue

Cite this: *RSC Adv.*, 2022, **12**, 9793

Larvicidal and histopathological efficacy of cinnamic acid analogues: a novel strategy to reduce the dengue vector competence

P. Naresh,[a] R. Rajesh Kumar,[b] H. N. Vishwas,[c] Gopalan Rajagopal,[d] T. Prabha[e] and S. Jubie *[a]

Received 31st December 2021
Accepted 14th March 2022

DOI: 10.1039/d1ra09466a

rsc.li/rsc-advances

Background: A novel strategy such as conjugation of amino, Schiff's bases, and thiadiazole moieties to the cinnamic acid nucleus has been adopted in this study to discover new molecules that target the dengue envelope protein (DENVE). *Aim*: Among the different domains of dengue virus envelope protein (PDB ID 1OKE), we have selected a ligand-binding domain for our structure-based drug design. The designed compounds have also been docked against DENVE protein. *Methodology*: Based on the *in silico* results and synthetic feasibility, three different schemes were used to synthesize twenty-three novel cinnamic acid derivatives. Sci-finder ascertained their novelty. The synthesized derivatives were consistent with their assigned spectra. The compounds were further evaluated for their larvicidal activity and histopathological analysis. Multiple linear regression analysis was performed to derive the QSAR model, which was further evaluated internally and externally for the prediction of activity. *Results and discussion:* Four compounds, namely CA 2, CA 14, ACA 4, and CATD 2, effectively showed larvicidal activity after 24, 48, and 72 h exposure; particularly, compound CA2 showed potent larvicidal activity with LC_{50} of 82.15 μg ml^{-1}, 65.34 μg ml^{-1}, and 38.68 μg ml^{-1}, respectively, whereas intermittent stages, causes of abscess in the gut, and siphon regions were observed through histopathological studies. *Conclusion*: Our study identified some novel chemical scaffolds as effective DENVE inhibitors with efficacious anticipated pharmacokinetic profiles, which can be modified further.

1. Introduction

The primary carrier of viruses that cause dengue fever, *Aedes aegypti*, is found in vast areas of the tropics and subtropics. There are currently no known therapies for dengue fever. However, standard fever treatment is available (nursing care, fluid balance, electrolytes, and blood clotting parameters). As a result, the only way to reduce the prevalence of this disease is by mosquito management, which involves interrupting the disease propagation cycle by attacking mosquito larvae at breeding sites. Besides vector control, a recently authorized dengue vaccine immunizes against all four serotypes. Dengvaxia is Sanofi Pasteur's (Paris, France) chimeric yellow fever-dengue-tetravalent dengue vaccine (CYD-TDV), the first and only of its type, and has been registered for use in 19 countries but is only available in 10.2 of them. In addition, several phase II and phase III trials have resulted in specific vaccine restrictions, such as CYD TDV being delivered exclusively to those who have previously been infected with dengue and live in endemic regions.[13–16]

Presently around the world, dengue is endemic in 112 countries.[1,2] Mostly in tropical and subtropical areas, each year, 50–100 million individuals are infected with DENV, resulting in nearly 500 000 severe life-threatening illnesses and 25 000 deaths.[3,4] One attractive approach could be the interruption of the virus replication at an early stage of attachment.[5] DENV enters the cell by receptor-mediated endocytosis followed by viral E protein-mediated membrane fusion. Membrane fusion is a major molecular event during viral entry into the host cell.[6] E (envelope) protein is a significant component of the virion surface, plays an essential role in binding to the host receptor, and assists virus fusion.[7] Among the three domains present in the E protein, the hinge region movement of domains I and II facilitates the fusion process.[8] Upon lowering the pH, the E protein undergoes significant conformational changes in the hinge region, springing upwards to bring the fusion peptide closer to the host membrane for fusion to occur. Small

[a]*Department of Pharmaceutical Chemistry, JSS College of Pharmacy, JSS Academy of Higher Education and Research, Ooty, Tamilnadu, India. E-mail: jubie@jssuni.edu.in; Web: https://www.jssuni.edu.in/*

[b]*Department of Pharmaceutical Biotechnology, JSS College of Pharmacy, JSS Academy of Higher Education and Research, Ooty, Tamilnadu, India*

[c]*Department of Pharmacy Practice, JSS College of Pharmacy, JSS Academy of Higher Education and Research, Ooty, Tamilnadu, India*

[d]*Postgraduate and Research Department of Zoology, Ayya Nadar Janaki Ammal College, Sivakasi, Tamilnadu, India*

[e]*Department of Pharmaceutical Chemistry, Nandha College of Pharmacy, Affiliated to The Tamilnadu Dr MGR Medical University-Chennai, Erode, Tamilnadu, India*

molecules' rearrangement and/or conformational changes in the hinge region may interrupt the fusion process.[9] A small detergent molecule, *n*-octyl-β-D-glucoside (βOG), occupies the hydrophobic pocket, which is located in the hinge region and plays a significant role in the rearrangement. It has been reported that mutations within this binding pocket lead to the alterations of the pH threshold for fusion. In addition to this, the protonation of histidine residues present in the hydrophobic domain would also impart the conformational change of the E protein. The previously reported fusion inhibitors such as peptidic antivirals suffer from poor absorption from the gastrointestinal tract, necessitating intravenous delivery and high manufacturing costs.[10] We, therefore, wanted to develop nonpeptidic small molecules to inhibit dengue virus entry.

While searching for small molecules, we came across an exciting scaffold, zosteric acid, isolated from marine eelgrass, *Zostera marina*. It has been reported that zosteric acid, chemically *p*-sulphoxycinnamic acid, and its analogs act as entry inhibitors by inhibiting the fusion process. Based on the reported antiviral potency of zosteric acid, we moved on to a similar readily available scaffold cinnamic acid, the naturally occurring precursor of flavonoids. It has excellent potential for a therapeutic role, showing antimicrobial, antifungal, and antitumor activities.[11] A compound derived from *trans*-cinnamic acid, *p*-sulphoxy-cinnamic acid, showed antiviral activity against the dengue virus, suggesting a possible antiviral potential of *trans*-cinnamic acid.[12] Besides, the modification of the –COOH group of cinnamic acid analogs leads to decreased IC_{50} values against DENV (Fig. 1). Keeping all facts in mind, the present work is aimed to identify novel bioactive molecules bearing cinnamic acid as a key signature of DENV entry.

2. Materials and methods

Sigma Aldrich, SD Fine, and Carbanio supplied all the chemicals used which were of analytical grade. The solvents were purified and dried by industry standards. The ^{1}H and ^{13}C NMR data were analyzed using a Bruker 400 MHZ spectrometer. The internal standard was tetramethyl silane (TMS), and the solvent was DMSO-d_6. Chemical shifts were reported downfield from TMS in parts per million (ppm). For analytical thin-layer chromatography, the plates used were MERCK aluminium back precoated silica gel 60-F 254 (0.5 mm) plates. An iodine chamber or UV light was used to identify the spots on TLC plates visually. Shimadzu recorded mass spectra.

2.1. *In silico* design

The ADME, molecular docking, and molecular dynamics studies were conducted using Discovery Studio (D.S.) 4.1 and PyRx 0.8. The MMGBSA assay was performed using Schrodinger 2017.2 and the 3D QSAR studies were performed using MOE 2009.10 software.[17] The preparation of protein (PDB ID 1OKE) and a library of seventy-two novel ligands was carried out by the standard method.[18–20] The CDOCKER module was used for calculating ligand binding affinity and energies.[21] The protein binding site was identified using existing ligands in the PDB database, and the sphere concept identified the location.[22] All other remaining procedure was followed and maintained by the reported methods.[23–25] The protein–ligand interactions were visualized and evaluated with DS 4.1.

PyRx 0.8 was used to perform the docking research of designed cinnamic acid analogues against FK506-binding protein (FKBP) from *Aedes aegypti* (PDB ID 3UQI). PyRx is

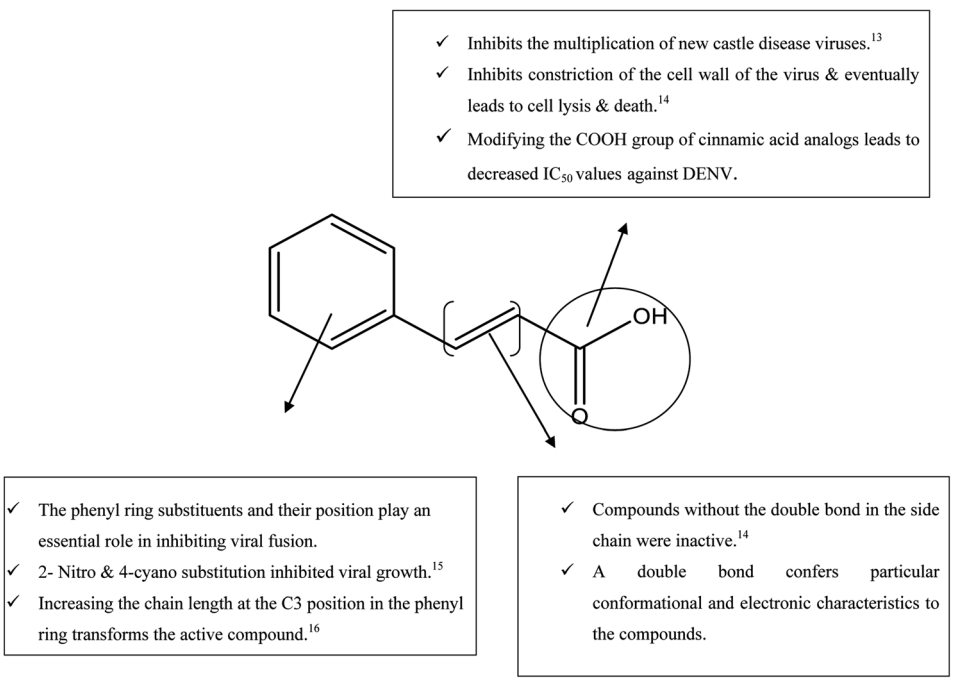

Fig. 1 SAR of cinnamic acid.

a Python-based programming language that runs on almost any modern machine, from personal computers to supercomputers. PyRx has been used to determine the binding affinity of a ligand for a protein to facilitate molecular docking. PyRx, a structure-based docking program, was used to screen cinnamic acid analogues for *Aedes aegypti* (PDB ID 3UQI) at a resolution of 1.30 Å. Additionally, ligands for energy reduction interact in good ways. The MMFF94 force field performed the minimization in 200 steps with an RMS gradient of 0.1. Following the devaluation, the ligands were transferred to the PDBQT format. First, we chose the macromolecule that will define the produced protein's binding site. Next, the active docking site was constructed utilizing bound ligand binding locations. Then, molecular docking was performed on a molecular window, with all produced ligands interacting with the specified active site.[34,35] First, all ligands were categorized according to their binding affinity as determined by the PyRx score. Following that, the ligands were classified according to their binding energy levels.

2.1.1. ADME studies. The ADME module of DS 4.1 was used to evaluate the compound's ADMET properties.[26]

2.1.2. Insecticide likeness studies. The designed cinnamic acid analogues were screened using the InsectiPAD database (Insecticide Physicochemical-properties Analysis Database), a unique agrochemical database to provide information of all approved insecticides, and qualitative and quantitative evaluation of insecticide likeness of small molecules.

2.2. Chemistry

Twenty-three acid analogues were selected from a library of seventy-two cinnamic acid derivatives that showed significant *in silico* results and were synthetically feasible.

2.2.1. General procedure for the synthesis of amino cinnamic acid hydrazides (ACA 1–4). The 4-amino cinnamic acid (40 mmol, 5.2 g) in acetonitrile with a coupling reagent *N*,*N*-dicyclohexyl carbodiimide (48 mmol, 80 ml) has been used in the presence of hydroxy benzotriazole (48 mmol, 9.98 g) (HOBT). The reaction mixture was stirred at room temperature for ten h, and the reaction process was monitored by TLC to obtain the 4-amino cinnamic acid ester (ACE). To the dried ACE, different hydrazines (3.8 mmol) in acetonitrile were added consecutively with stirring at 0 °C and 5 °C for one h and at R.T. for five h. Then, the obtained dicyclohexyl urea (DCU) was removed by filtration, and the filtrate was allowed to stand at 0 °C overnight and filtered again (Scheme 1).

2.2.1.1. (2E)-3-(4-Aminophenyl)-N′-(2,4-dinitrophenyl)prop-2-enehydrazide (ACA 1). Green solid; Rf value = 0.52 (*n*-hexane : ethyl acetate, 6 : 4, v/v developer, visualization: UV and I_2),

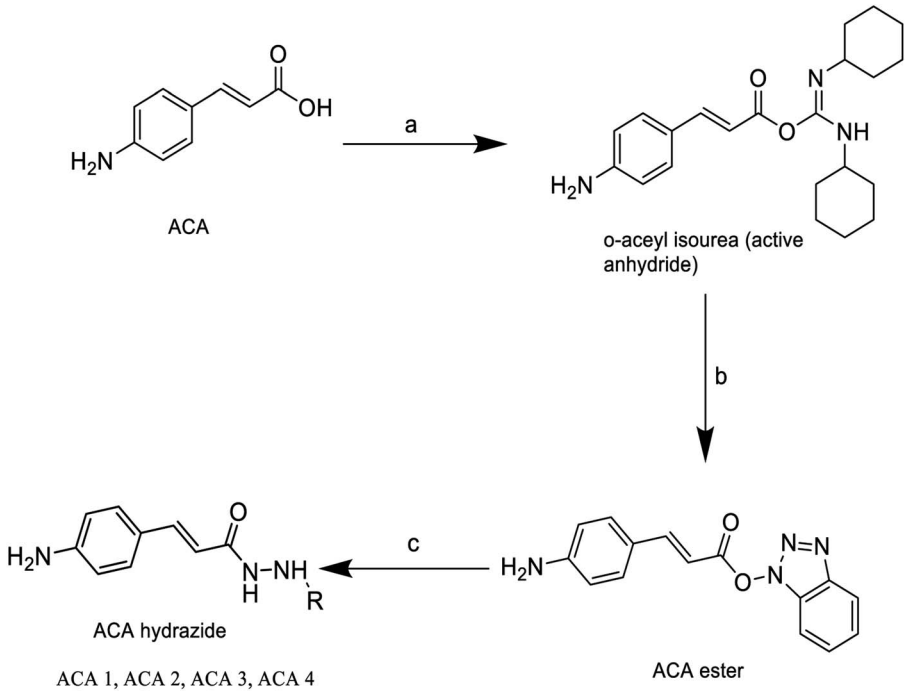

	R
ACA 1	$C_{15}H_{13}N_5O_5$
ACA 2	$C_9H_{11}N_3O$
ACA 3	$C_{10}H_{12}N_4OS$
ACA 4	$C_{17}H_{16}BrN_3O_2$

Scheme 1 Synthesis of amino cinnamic acid hydrazide derivatives. Reagents and conditions, (a) catalytic DCC (dicyclohexyl carbodiimide). (b) HOBt (1-hydroxy benzotriazole), CH_3CN (acetonitrile), stir at room temperature overnight. (c) Different hydrazines, CH_3CN, stir overnight at room temperature.

yield 85%. Mp. 268–270 °C. M.F. $C_{15}H_{13}N_5O_5$; MW: 343.25 FTIR (KBr, cm^{-1}) 3423.12 (NH_2 str), 3297.48 (C–NH str), 3282.35 (C–NH str), 2892.72 (CH str Ar), 2853.58 (CH str Ali), 1656.05 (C=O), 1264.54 (C–N str). ^{1}H NMR (300 MHz, DMSO) δ 5.84 (s, 2H, NH_2), 7.35–7.62 (m, 4H, Ar H), 7.30–7.45 (m, 3H, Ar H), 9.32 (t, 2H, NH), 9.90 (d, J = 6.3 Hz, 2H, NH_2), 5.91 (d, J = 6.3 Hz, 2H, CH), 6.96 (d, J = 6.3 Hz, 2H, CH). ^{13}C NMR (300 MHz, DMSO) δ 114.25, 114.86, 115.00, 121.03, 124.81, 129.40, 129.65, 130.21, 134.52, 139.60, 141.25, 147.46, 152.8, 162.49, 165.80 (aryl carbons), 115.46, 140.15 (CH=CH), 163.21 (C–NH). MS (M–H): 343.20; 146.16 (C_9H_8NO m/z), 155.01 ($C_5H_3N_2O_4$ m/z +1), ($C_7H_6BrN_2O$ m/z).

2.2.1.2. 2-[(2E)-3-(4-Aminophenyl)prop-2-enoyl]hydrazine-1-carbothioamide (ACA 3). Ash solid; Rf value = 0.64 (*n*-hexane : ethyl acetate, 6 : 4, v/v developer, visualization: UV and I_2), yield 81%. Mp. 264–266 °C. M.F. $C_{10}H_{12}N_4O_5$; MW: 236.15 FTIR (KBr, cm^{-1}) 3330.23 (NH_2 str), 3218.32 (C–NH str), 3033.16 (C–NH str), 2929.97 (CH str Ar), 2854.63 (CH str Ali), 1623.90 (C=O), 1783.21 (C=N), 1242.24 (C–N str), 1173.72 (C=S str). ^{1}H NMR (300 MHz, DMSO) δ 5.23 (s, 2H, NH_2), 6.31–7.62 (m, 4H, Ar H), 9.15 (d, J = 6.3 Hz, 1H, NH), 8.44 (d, 1H, NH), 6.12 (s, H, NH_2), 6.67 (d, J = 6.5 Hz, 2H, CH), 6.44 (d, J = 6.5 Hz, 2H, CH). ^{13}C NMR (300 MHz, DMSO) δ 113.27, 114.52, 123.50, 127.29, 129.60, 134.62 (aryl carbons), 120.84, 142.12 (CH=CH), 178.45 (C=S), 162.42 (CO NH). MS (M–H): 236.28; 115.89 (C_8H_8N m/z), 90.12 (CH_4N_3S m/z +5), 118.21 ($C_2H_4N_3OS$ m/z +4).

2.2.1.3. (2E)-3-(4-Aminophenyl)-N′-(2,4-dinitrophenyl)prop-2-enehydrazide (ACA 4). Brown solid; Rf value = 0.58 (*n*-hexane : ethyl acetate, 6 : 4, v/v developer, visualization: UV and I_2), yield 88%. Mp. 278–280 °C. M.F. $C_{16}H_{14}BrN_3O_2$; MW: 360.20 FTIR (KBr, cm^{-1}) 3472.52 (NH_2 str), 3372.65 (C–NH str), 2931.90 (CH str Ar), 2851.85 (CH str Ali), 1681.02 (C=O), 1342.52 (C–N str), 523.34 (C–Br str). ^{1}H NMR (300 MHz, DMSO) δ 4.84 (s, 2H, NH_2), 7.4 (m, 4H, Ar H), 7.2 (m, 4H, Ar H), 7.9 (d, J = 7.5 Hz, H, NH), 7.6 (d, J = 7.5 Hz, H, NH), 6.65 (d, J = 7.5 Hz 2H, CH), 6.5 (d, J = 7.5 Hz 2H, CH). ^{13}C NMR (300 MHz, DMSO) δ 112.36, 113.29, 118.47, 121.07, 122.41, 125.39, 127.37, 128.34, 128.94, 129.73, 133.30, and 140.56 (aryl carbons), 110.24, 135.15 (CH=CH), 163.19, 164.47 (CO NH). MS (M–H): 360.20; 115.89 (C_8H_8N m/z), 182.01 (C_7H_4BrO m/z −1), ($C_7H_6BrN_2O$ m/z).

2.2.2. Synthesis of cinnamic acid-triazole. A mixture of the carbon disulfide (0.015 mmol, 14 ml), potassium hydroxide (0.015 mmol, 8.4 g) in 100 ml of 99% ethanol, and cinnamic acid hydrazide (0.01 mmol, 1.62 g) was stirred for 20 h. Dry ether (150 ml) was added to the resulting mixture, and the precipitate potassium dithiocarbazinate was collected by filtration (Scheme 2). The obtained potassium salt (0.015 mmol, 4.4 g), hydrazine hydrate (2 ml), and distilled water (10 ml) mixture were refluxed with stirring to obtain the white residue on cooling. Then the concentrated hydrochloric acid was used to acidify, followed by filtration to obtain the desired product, which was recrystallized with ethanol.

2.2.3. General procedure for the synthesis of Schiff bases (CA 1–14). Equimolar mixtures of 1,2,4-triazole obtained from Scheme 2 with various aromatic aldehydes and a catalytic amount of 3–5 drops of concentrated sulphuric acid were refluxed in an ethanol medium for 5–8 h. The resultant was cooled to room temperature; the sediment solid was filtered and recrystallized in hot ethanol.

2.2.3.1. 2-{[(4-Chlorophenyl) methylidene] amino}-1-[(E)-2-phenylethenyl]-2,5-dihydro-1H-1,2,4-triazole-3-thiol (CA 1). Yellow solid; Rf value = 0.62 (*n*-hexane : ethyl acetate, 6 : 4, v/v developer, visualization: UV and I_2), yield 83%. Mp. 240–242 °C. M.F. $C_{17}H_{15}N_5O_2S$; MW: 352.39 FTIR (KBr, cm^{-1}) 3087.17 (CH Ar), 2927.08 (CH Ali), 2284.25 (C–S str), 1700.31 (C=N str), 1268.24 (C–N str) 970.23 (N–C–S str), 806.27 (Ar CH), 370.34 (C–Cl). ^{1}H NMR (300 MHz, DMSO) δ 8.34–8.35 (m, 5H, Ar H), 8.32–8.33 (m, 4H, Ar H), 8.72 (s, N=CH), 6.9 (d, J = 6.2 Hz, 2H, CH), 6.2 (d, J = 6.2 Hz, 2H, CH), 3.40 (s, 2H, CH_2), 1.51 (s, H, SH). ^{13}C NMR (300 MHz, DMSO) δ 112.25, 116.48, 121.32, 123.25, 125.79, 128.81, 129.93, 134.17, 135.49, 137.25, 140.41, 141.15 (aryl carbons), 64.35 (CH_2), 116.23, 132.58 (CH=CH), 148.69 (N=C), 160.38 (C=N, imine). MS (M–H): 352.39 (m/z +2); 103.24 (C_8H_7 m/z), 203.15 ($C_{10}H_{10}N_3S$ m/z +1), 149.32 ($C_7H_5N_2O_2$ m/z).

2.2.3.2. 4-[({2-[(E)-2-Phenylethenyl]-5-sulfanyl-2,3-dihydro-1H-1,2,4-triazol-1-yl}imino)methyl] phenol (CA 2). Milky solid; Rf value = 0.36 (*n*-hexane : ethyl acetate, 6 : 4, v/v developer, visualization: UV and I_2), yield 80%. Mp. 268–270 °C. M.F. $C_{17}H_{16}N_4OS$; MW: 322.38 FTIR (KBr, cm^{-1}) 3177.58 (OH str), 3019.66 (CH str Ar), 2957.94 (CH str Ali), 2363.84 (C–S), 1600.97 (C=N str), 1240.27 (C–N str), 973.93 (N–C–S str), 816.88 (Ar CH str). ^{1}H NMR (300 MHz, DMSO) δ 10.63 (s, H, OH), 7.32–7.35 (m, 5H, Ar H), 7.56–7.59 (m, 4H, Ar H), 8.72 (s, H, N=CH), 6.9 (d, J = 6.2 Hz, 2H, CH), 6.2 (d, J = 6.2 Hz, 2H, CH), 3.50 (s, 2H, CH_2), 1.41 (s, H, SH). ^{13}C NMR (300 MHz, DMSO) δ 112.21, 118.24, 120.21, 122.38, 124.25, 125.26, 127.60, 128.35, 130.12, 133.35, 133.59, 142.40 (aryl carbons), 70.15 (CH_2), 116.54, 130.87 (CH=CH), 141.15 (N=C), 159.16 (C=N). MS (M–H): 324.40 (m/z +2); 103.14 (C_8H_7 m/z), 203.11 ($C_{10}H_{10}N_3S$ m/z +1), 125.21 (C_7H_6NO m/z).

2.2.3.3. 2-{[(4-Chlorophenyl) methylidene] amino}-1-[(E)-2-phenylethenyl]-2,5-dihydro-1H-1,2,4-triazole-3-thiol (CA 3). White solid; Rf value = 0.42 (*n*-hexane : ethyl acetate, 6 : 4, v/v developer, visualization: UV and I_2), yield 80%. Mp. 221–223 °C. M.F. $C_{17}H_{15}ClN_4S$; MW: 340.82 FTIR (KBr, cm^{-1}) 3173.01 (CH str Ar), 2991.69 (CH str), 2917.43 (CH str Ali), 2349.38 (C–S str), 1700.97 (C=N str), 1274.03 (C–N str), 947.08 (N–C–S), 826.88 (Ar CH str). ^{1}H NMR (300 MHz, DMSO) δ 7.85–7.89 (m, 5H, Ar H), 7.47–7.49 (m, 4H, Ar H), 8.5 (s, H, N=CH), 6.90 (d, J = 6.3 Hz, H, CH), 6.20 (d, J = 6.3 Hz, H, CH), 3.22 (s, 2H, CH_2), 1.50 (s, H, CH). ^{13}C NMR (300 MHz, DMSO) δ 113.52, 114.25, 115.13, 117.48, 120.21, 121.89, 122.10, 123.35, 124.80, 125.50, 127.28, 128.52 (aryl carbons) 72.58 (CH_2), 120.14, 138.45 (CH=CH), 142.90 (N=C), 172.23 (C=N). MS (M–H): 342.84 (m/z +1); 144.28 (C_7H_5ClN m/z −1), 206.77 ($C_{10}H_{10}N_3S$ m/z −2).

2.2.3.4. 1-[(E)-2-Phenylethenyl]-2-{[(3,4,5-trimethoxy phenyl) methylidene] amino}-2,5-dihydro-1H-1,2,4-triazole-3-thiol (CA 5). Pinky solid; Rf value = 0.47 (*n*-hexane : ethyl acetate, 6 : 4, v/v developer, visualization: UV and I_2), yield 91%. Mp. 220–222 °C. M.F. $C_{20}H_{22}N_4O_3S$; MW: 396.46 FTIR (KBr, cm^{-1}) 3063.06 (CH str Ar), 2987.89 (CH str), 2917.43 (CH str Ali), 2118.87 (C–S str), 1692.59 (C=N str), 1232.55 (C–N str), 948.04 (N–C–S str), 846.88 (Ar CH str). ^{1}H NMR (300 MHz, DMSO) δ 8.42–8.57 (m, 5H, Ar H), 7.08–7.26 (m, 4H, Ar H), 3.93 (s, 9H,

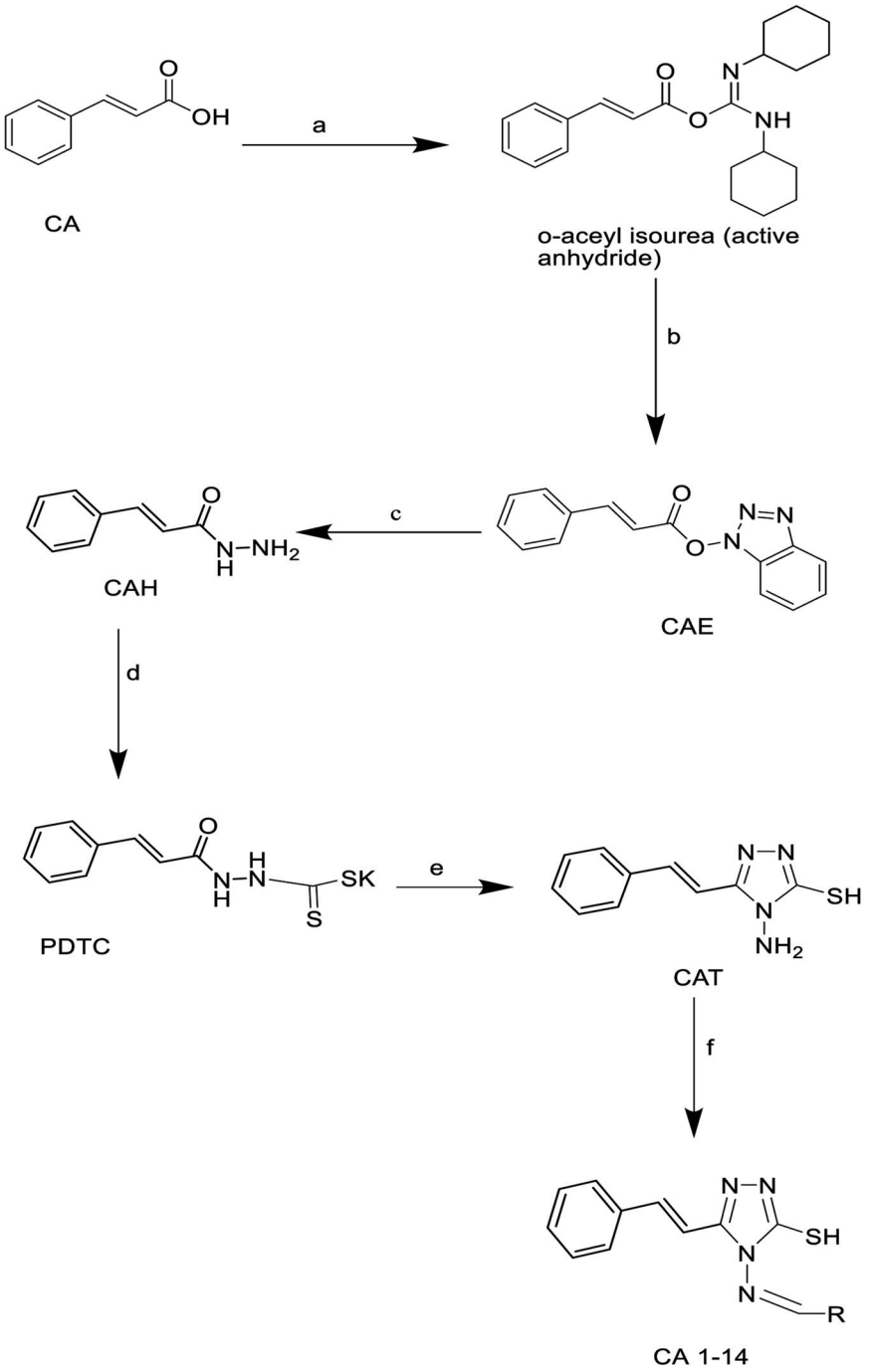

	R				
CA 1	$C_{17}H_{15}N_5O_2S$	CA 6	$C_{19}H_{21}N_5S$	CA 11	$C_{21}H_{23}N_5S$
CA 2	$C_{17}H_{16}N_4OS$	CA 7	$C_{18}H_{18}N_4O_2S$	CA 12	$C_{18}H_{18}N_4OS$
CA 3	$C_{17}H_{15}ClN_4S$	CA 8	$C_{17}H_{16}N_4O_2S$	CA 13	$C_{17}H_{16}N_4OS$
CA 4	$C_{17}H_{14}Cl_2N_4S$	CA 9	$C_{17}H_{15}N_5O_2S$	CA 14	$C_{17}H_{15}N_5O_2S$
CA 5	$C_{20}H_{22}N_4O_2S$	CA 10	$C_{17}H_{15}BrN_4S$		

Scheme 2 Synthesis of cinnamic acid derivatives. Reagent conditions, (a) catalytic DCC (dicyclohexyl carbodiimide). (b) HOBt (1-hydroxy benzotriazole), CH_3CN (acetonitrile), overnight at room temperature, stir. (c) $NH_2NH_2H_2O$ (hydrazine hydrate), CH_3CN (acetonitrile), overnight at room temperature, stir. (d) KOH (potassium hydroxide), CS_2 (carbon disulfide), ethanol, stir overnight at room temperature. (e) $NH_2NH_2H_2O$ (hydrazine hydrate), H_2O, reflux for ten h. (f) Benzaldehyde, ethanol, conc. H_2SO_4, reflux for 3 h.

CH_3), 6.20 (d, J = 6.6 Hz, H, CH), 5.08 (d, J = 6.6 Hz, H, CH), 1.53 (s, H, SH). ^{13}C NMR (300 MHz, DMSO) δ 110.52, 111.22, 112.23, 114.05, 115.15, 116.26, 117.72, 119.28, 120.38, 128.18, 129.45, 131.27 (aryl carbons), 71.28 (CH_2), 60.91, 56.32, 56.11 (O–CH_3), 115.24, 139.43 (CH=CH), 140.82 (N=C), 161.51 (C=N, imine). MS (M–H): 398.47 (m/z +2); 101.13 ($C_2H_3N_3S$ m/z −2); 106.38 (C_8H_7 m/z −3); 189.57 ($C_{10}H_{12}NO_3$ m/z +2).

2.2.3.5. 2-Methoxy-4-[({2-[(E)-2-phenylethenyl]-5-sulfanyl-2,3-dihydro-1H-1,2,4-triazol-1-yl} imino) methyl] phenol (CA 7). Brown solid; Rf value = 0.46 (*n*-hexane : ethyl acetate, 6 : 4, v/v developer, visualization: UV and I_2), yield 85%. Mp. 236–238 °C. M.F. $C_{18}H_{18}N_4O_2S$; MW: 354.41 FTIR (KBr, cm^{-1}) 3336.00 (OH str), 3197.23 (CH str Ar), 2973.37 (CH str Ali), 2371.56 (C–S str), 1647.26 (C=N str), 1240.27 (C–N str), 977.54 (N–C–S str), 851.60 (Ar CH str). ^{1}H NMR (300 MHz, DMSO) δ 7.33–7.60 (m, 5H, Ar H), 6.24–6.27 (m, 3H, Ar H), 10.23 (s, H, OH), 8.25 (s, H, N=CH), 3.00 (S, 2H, CH_2), 3.65 (S, 3H, CH_3), 1.62 (s, H, SH). ^{13}C NMR (300 MHz, DMSO) δ 112.01, 115.52, 117.13, 119.44, 122.92, 128.53, 130.90, 133.38, 134.24, 135.82, 136.41, 140.27 (aryl carbons), 56.55, 54.12, 54.84 (O–CH_3), 20.24, 130.87 (CH=CH), 169.64 (C=N). MS (M–H): 354.42 (m/z +2); 144.34 ($C_8H_8NO_2$ m/z +); 204.27 ($C_{10}H_{10}N_3S$ m/z +); 251.28 ($C_{10}H_{11}N_4O_2S$ m/z).

2.2.3.6. 2-{[(4-Nitrophenyl) methylidene] amino}-1-[(E)-2-phenylethenyl]-2,5-dihydro-1H-1,2,4-triazole-3-thiol (CA 9). Blue solid; Rf value = 0.56 (*n*-hexane : ethyl acetate, 6 : 4, v/v developer, visualization: UV and I_2), yield 87%. Mp. 240–242 °C. M.F. $C_{17}H_{15}N_5O_2S$; MW: 353.39 FTIR (KBr, cm^{-1} 3103.57) (CH str Ar), 3044.74 (CH str Ar), 2946.36 (CH str Ali), 2359.98 (C–S str), 1636.65 (C=N str), 1264.38 (C–N str), 960.85 (N–C–S str), 853.53 (Ar CH str). ^{1}H NMR (300 MHz, DMSO) δ 8.14–8.28 (m, 5H, ArH), 7.24–7.39 (m, 4H, ArH), 8.44 (s, H, N=CH), 6.12 (d, J = 6.8 Hz, H, CH), 5.25 (d, J = 6.8 Hz, H, CH), 3.31 (s, 2H, CH_2)1.58 (s, H, SH). ^{13}C NMR (300 MHz, DMSO) δ 116.15, 120.24, 122.31, 124.01, 124.27, 126.14, 128.01, 130.29, 132.57, 134.92, 136.49, 136.48 (aryl carbons), 74.15 (CH_2), 119.87, 136.87 (CH=CH), 144.68 (N=C), 161.10 (C=N, imine). MS (M–H): 353.39 (m/z +1); 149.12 ($C_7H_5N_2O_2$ m/z −2); 204.37 ($C_{10}H_{10}N_3S$ m/z +1); 250.25 ($C_9H_8N_5O_2S$ m/z).

2.2.3.7. 2-{[(4-Bromophenyl) methylidene] amino}-1-[(E)-2-phenylethenyl]-2,5-dihydro-1H-1,2,4-triazole-3-thiol (CA 10). Brown solid; Rf value = 0.41 (*n*-hexane : ethyl acetate, 6 : 4, v/v developer, visualization: UV and I_2), yield 94%. Mp. 252–254 °C. M.F. $C_{17}H_{15}BrN_4S$; MW: 387.29 FTIR (KBr, cm^{-3} 123.57) (CH str Ar), 2905.31 (CH str Ali), 2315.54 (C–S str), 1636.65 (C=N str), 1231.48 (C–N str), 961.47 (N–C–S str), 813.35 (Ar CH str). ^{1}H NMR (300 MHz, DMSO) δ 8.14–8.28 (m, 5H, Ar H), 7.24–7.39 (m, 4H, Ar H), 8.44 (s, H, N=CH), 6.10 (d, J = 6.7 Hz, H, CH), 5.17 (d, J = 6.7 Hz H, CH), 2.92 (s, 2H, CH_2),1.38 (s, H, SH). ^{13}C NMR (300 MHz, DMSO) δ 116.15, 122.33, 125.31, 128.00, 129.89, 130.16, 131.48, 134.25, 134.54, 136.45, 142.12 (aryl carbons), 69.18 (CH_2), 121.24, 135.54 (CH=CH),141.19 (N=C), 163.41 (C=N, imine). MS (M–H): 387.29 (m/z +2); 101.16 ($C_2H_3N_3S$ m/z); 183.02 (C_7H_5BrN m/z +2); 289.15 ($C_9H_8BrN_4S$ m/z).

2.2.3.8. 2-({(2E)-3-[4-(Dimethylamino)phenyl]prop-2-en-1-ylidene} amino)-1-[(E)-2-phenylethenyl]-2,5-dihydro-1H-1,2,4-triazole-3-thiol (CA 11). Brown solid; Rf value = 0.41 (*n*-hexane : ethyl acetate, 6 : 4, v/v developer, visualization: UV and I_2), yield 90%. Mp. 246–248 °C. M.F. $C_{21}H_{23}N_5S$; MW: 377.50 FTIR (KBr, cm^{-3} 2811.34) (CH str Ar), 2361.91 (C–S str), 1636.65 (C=N str), 1378.18 (C–N str), 966.38 (N–C–S str), 868.36 (Ar CH str). ^{1}H NMR (300 MHz, DMSO) δ 7.26–7.67 (m, 5H, Ar H), 6.33–7.05 (m, 4H, Ar H), 8.10 (s, H, N=CH), 6.02 (d, J = 6.9 Hz, H, CH), 5.35(d, J = 6.9 Hz, H, CH), 2.92 (s, 2H, CH_2), 3.21, 3.18 (s, 6H, CH_3), 1.58 (s, H, SH). ^{13}C NMR (300 MHz, DMSO) δ 112.25, 116.81, 119.28, 120.12, 123.56, 120.17, 126.49, 128.51, 129.17, 130.26, 130.92, 131.25 (aryl carbons), 65.39 (CH_2), 122.42, 138.32 (CH=CH), 137.24 (N=C), 167.32 (C=N, imine). MS (M–H): 377.50 (m/z +2); 173.23 ($C_{11}H_{13}N_2$ m/z −2); 207.42 ($C_{10}H_{10}N_3S$ m/z +1).

2.2.4. General procedure for the synthesis of 3,6-(substituted phenyl)-(1,2,4) triazolo (3,4-*b*) (1,3,4) thiadiazole. An equimolar quantity of 1,2,4-triazole with substituted benzoic acid in $POCl_3$ (5 ml) was refluxed with stirring for 4–5 h. Then the reaction mixture was slowly poured into crushed ice and neutralized with solid sodium bicarbonate. The resultant product was recrystallized with chloroform (Scheme 3).

2.2.4.1. 2-(3-Methylphenyl)-5-[(E)-2-phenylethenyl]-5,6-dihydro[1,2,4]triazolo[5,1-b][1,3,4]thiadiazole (CATD 2). White solid; retention factor (Rf) value = 0.68 (ethyl acetate : *n*-hexane,

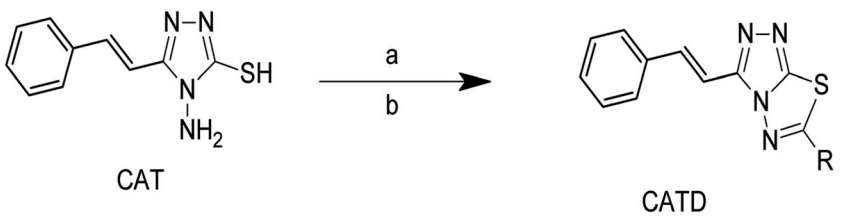

CAT CATD

R	
CATD 1	$C_{17}H_{15}N_5S$
CATD 2	$C_{18}H_{18}N_4S$
CATD 3	$C_{17}H_{14}N_4O_2S$
CATD 4	$C_{17}H_{13}N_5O_2S$
CATD 5	$C_{17}H_{13}ClN_4S$

Scheme 3 Synthesis of cinnamic acid thiadiazole derivatives. Reagent conditions, (a) 4-amino benzoic acid. (b) $POCl_3$, reflux for three h.

4 : 6, v/v developer, visualization: UV and I_2), yield 90%. Mp. 225–227 °C. M.F. $C_{18}H_{16}N_4S$; MW: 320.41 FTIR (KBr, cm^{-1}) 2923.22 (CH str Ar), 2827.34 (CH str Ali), 1163.11 (C–S str), 1603.86 (C=N str), 1247.99 (C–N str), N–C–S (962.54 str), 782.16 (Ar str CH). ^{1}H NMR (300 MHz, DMSO) δ 7.23–7.62 (m, 5H, Ar H), 7.42–7.55 (m, 4H, Ar H), 3.20 (s, H, CH_2), 2.42 (T, 3H, CH_3), 5.32 (d, $J = 6.3$ Hz, 2H, CH), 6.45 (d, $J = 6.3$ Hz, H, CH). ^{13}C NMR (300 MHz, DMSO) δ 124.12, 125.45, 126.20, 127.92, 128.52, 130.12, 131.50, 131.35, 133.56, 136.59, 138.82 (aryl carbons), 71.56 (CH_2), 115.82, 131.70 (CH=CH), 140.12, 156.70 (C=N, imine), 20.81 (CH_3). MS (M–H): 320.42 (m/z +2); 103.14 (C_8 H_7 m/z +1); 229.14 ($C_{11}H_9N_4S$ m/z +1), 91.13 (C_7H_7 m/z −1).

2.2.4.2. 4-{5-[(E)-2-Phenylethenyl]-5,6-dihydro[1,2,4]triazolo [5,1-b][1,3,4]thiadiazol-2-yl}benzene-1,2-diol (CATD 3). Brown solid; retention factor (Rf) value = 0.47 (ethyl acetate : *n*-hexane, 4 : 6, v/v developer, visualization: UV and I_2), yield 92%. Mp. 245–247 °C. M.F. $C_{17}H_{14}N_4O_2S$; MW: 338.38 FTIR (KBr, cm^{-1}) 3086.23 (CH str Ar), 2917.43 (CH str Ali), 2351.65 (C–S str), 1638.58 (C=N str), 1237.38 (C–N str), N–C–S (979.87 str), 830.38 (Ar str CH). ^{1}H NMR (300 MHz, DMSO) δ 7.2–7.5 (m, 5H, Ar H), 7.06–7.25 (m, 3H, Ar H), 9.01 (s, H, OH), 9.12 (s, H, OH), 8.34 (s, H, N=CH), 6.10 (d, $J = 6$ Hz, H, CH), 5.52 (d, $J = 6$ Hz, H, CH), 2.95 (s, 2H, CH_2), 1.45 (s, H, SH). ^{13}C NMR (300 MHz, DMSO) δ 110.29, 114.41, 118.52, 120.28, 123.20, 124.61, 126.31, 128.61, 129.54, 130.12, 131.47, 131.87 (aryl carbons), 73.18 (CH_2), 124.87, 137.29 (CH=CH), 148.08 (C–OH), 171.57 (C=N, imine). MS (M–H): 338.38 (m/z +2); 105.31 (C_8 H_7 m/z −2); 235.44 ($C_9H_7N_4O_2S$ m/z +1), 109.31 ($C_6H_5O_2$ m/z).

2.2.4.3. 2-(3-Methylphenyl)-5-[(E)-2-phenylethenyl]-5,6-dihydro[1,2,4]triazolo[5,1-b][1,3,4]thia diazole (CATD 4). Yellow solid; retention factor (Rf) value = 0.62 (ethyl acetate : *n*-hexane, 4 : 6, v/v developer, visualization: UV and I_2), yield 89%. Mp. 262–265 °C. M.F. $C_{17}H_{13}N_5O_2S$; MW: 351.38 FTIR (KBr, cm^{-1}) 3096.82 (CH str Ar), 2921.29 (CH str Ali), 1157.94 (C–S str), 1681.02 (C=N str), 1277.88 (C–N str), N–C–S (979.87 str), 832.31 (Ar str CH). ^{1}H NMR (300 MHz, DMSO) δ 7.39–7.68 (m, 5H, Ar H), 8.07–8.21 (m, 4H, Ar H), 1.52 (s, H, SH), 3.2 (d, 2H, CH_2), 6.41 (d, $J = 6.2$ Hz, H, CH), 5.37 (d, $J = 6.2$ Hz H, CH). ^{13}C NMR (300 MHz, DMSO) δ 122.01, 126.52, 127.32, 128.50, 128.87, 130.76, 131.26, 133.58, 134.69, 136.20, 138.51, 14.30 (aryl carbons), 70.54 (CH_2), 110.55, 134.42 (CH=CH), 143.20, 156.28 (C=N, imine). MS (M–H): 351.38 (m/z +2); 105.31 (C_8 H_7 m/z −2); 235.44 ($C_9H_7N_4O_2S$ m/z +1), 109.31 ($C_6H_5O_2$ m/z).

2.3. Biological activity

2.3.1. *In vitro* cytotoxicity assay. The *in vitro* cytotoxicity assay was performed by the reported method (27). The mitochondrial enzyme succinate dehydrogenase cleaves the tetrazolium salt MTT into a blue coloured substance (formazan). The number of cells used was discovered to be equal to the amount of formazan produced by the cells used.[27]

$$\text{Percentage of cell viability} = \frac{\text{Mean O.D. of individual test group} \times 100}{\text{Mean O.D. of the control group}}$$

2.3.2. Haemolytic assay. The synthesized compounds in fresh anti-coagulated human blood cells were centrifuged for 10 min at 2000 rpm, following which the cell pellets were resuspended in NaCl 0.9% to prepare a 2% v/v cell suspension. Next, the red blood cell suspension (100 μl) was added to a 96-well plate and incubated for one h at 37 °C in 5% CO_2. As an index of red blood cell lysis, the release of haemoglobin was determined spectrophotometrically at 540 nm. The complete hemolysis (positive control) was achieved by adding 1% (v/v) NaOH, while cells in 0.9% (w/v) NaCl solution served as a negative control.[28] The percentage of hemolysis was calculated as

$$(\%)\ \text{of hemolysis} = \frac{\text{Absorbance of the sample treated} - \text{absorbance of positive} \times 100}{\text{The absorbance of positive} - \text{absorbance of negative}}$$

2.3.3. Larvicidal bioassay. The larvicidal bioassay was assessed in the third stage instar larvae of *Aedes aegypti* following the standard World Health Organization larval susceptibility test method with minor modifications.[29] The synthesized compounds at concentrations ranging from 50 to 250 μg ml^{-1} were mixed with 50 ml of dechlorinated sterile water and 25 larvae were used in this assay. After 24, 48, and 72 h, the mortality of *Aedes Aegypti* larvae was determined, respectively. The infected larvae were examined under a stereo zoom microscope, and these were done in triplicate.

After larval exposure to test compounds after 24 hours and 48 hours, mortality was noted. The LC_{50} and LC_{90} values were further determined with the help of probit regression analysis. In addition, the chi-square value, degree of freedom, and *p*-value were documented. All the analysis was performed using SPSS 16. Any '*p*'-value <0.05 was considered statistically significant. The mortality of the larvae did not exceed 10% in the

control group. Hence, the present data did not require any additional statistical analysis.

2.3.4. Histopathological analysis. Following alcohol wash to harden the tissue, the larval samples were embedded in paraffin wax and subsequently sectioned (2 μm) using a microtome (Weswox Optik-1090A). The sections were mounted, and stained with eosin and hematoxylin, and different cells were visualized at 10× and 40× magnifications under a stereomicroscope.[30]

2.4. QSAR studies

The half-maximal lethal concentration (LC_{50}) measures the effectiveness of a substance in inhibiting a specific biological or biochemical function. The LC_{50} values were manually converted into pLC_{50} (predicted LC_{50}) using the formula $pLC_{50} = -\log LC_{50}$. For performing the QSAR study, a dataset of 24 synthesized compounds was chosen, from which 19 training sets and 5 test set compounds were assigned accordingly. The seven descriptors were chosen to describe the structure of the compounds comprising the series to study *viz.*, dipole moment (AM1_dipole), molar refractivity (M.R.), lowest unoccupied molecular orbital (AM1_LUMO), partition coefficients (log *P*(o/w)), highest unoccupied molecular orbital (AM1_HOMO), van der Waals energies (EvdW), and topological polar surface area (TPSA).[31] The Multiple Linear Regression (MLR) procedures were used to create the QSAR model, which was constructed from the QSAR descriptor panel of the MOE 2009.10 suite,[32] and the RMSE and R^2 values were derived from the QSAR fit.[33] A QSAR correlation plot was generated by plotting the values of pLC_{50} on the *x*-axis and the predicted values ($PRED) on the *y*-axis for all the nineteen compounds (Fig. 9).

3. Results and discussion

3.1. *In silico* study of cinnamic acid analogues against DENVE (PDB ID 1OKE)

A compound library of seventy-two new substances substituted with various aldehydes and benzoic acids at the 2nd and 4th positions of cinnamic was designed (Table 1). The proposed compounds were postulated as new molecules by *Sci-finder* software.

The most effective ligand binding site was discovered in pocket number 26, which had a volume of 1178.9 $Å^3$ and an area of 901.1 $Å^2$. There are 26 amino acid residues in this pocket, including Thr 48, Glu 49, Ala 50, Lys 51, Gly 271, Leu 275, Thr 280, Lys 120, Ala 205, Lys 198, Val 130, Ala 53, Gly 280, Lys 275, Leu 191, and Arg 57 (Fig. 2). Our study found the same pocket

Table 1 Designed cinnamic acid analogues

Compounds	Pattern of substitution	Rationale
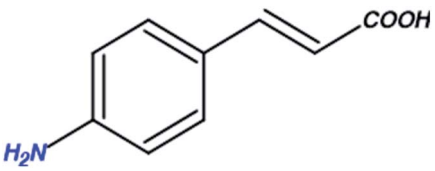	NH_2 substitution	To inhibit the viral growth
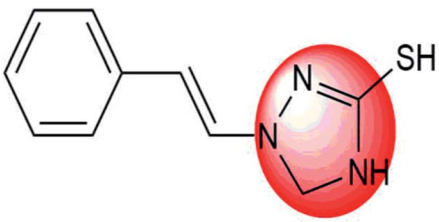	Modification of COOH group of 1,2,4-triazole scaffold	To decrease IC_{50} values against DENV
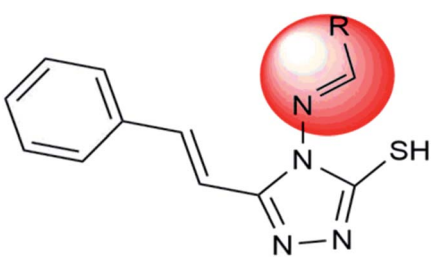	Addition of different aromatic aldehydes (2nd & 4th position) (Schiff's base) on the triazole ring	To inhibit the viral growth
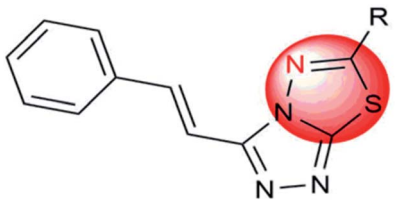	Thiadiazole substitution and its position	Play on a significant role in the inhibition of viral fusion

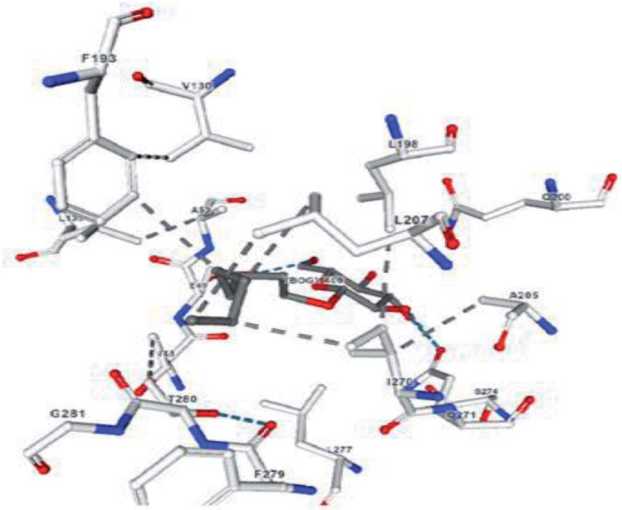

Fig. 2 Amino acid residues present in the active site of DENV envelope protein.

Table 2 Binding energies of cinnamic acid analogues against DENVE Protein (1OKE)

S. No.	Comp. name	C docker energy (−kcal mol^{-1})	C docker interaction energy (−kcal mol^{-1})
1	CA 1	31.9484	28.2893
2	CA 2	56.9833	45.5343
3	CA 3	37.9812	19.5848
4	CA 4	42.8537	34.7445
5	CA 5	38.8767	30.1751
6	CA 6	37.5519	35.706
7	CA 7	32.6039	35.2159
8	CA 8	42.3452	32.9779
9	CA 9	31.7342	36.3489
10	CA 10	35.3552	30.806
11	CA 11	30.8311	34.2838
12	CA 12	28.1112	36.826
13	CA 13	33.1193	32.1901
14	CA 14	36.65667	24.6668
15	ACA 1	39.36247	31.4295

with the above amino acid residues, and the Ramachandran plot further validated the prepared protein (Fig. 3). In addition, the CDOCKER energy of the synthesized compounds was lower than that of the reference inhibitor P02 (−132.553), as shown in Table 2, indicating that these molecules may have a higher binding affinity for DENVE (Fig. 4).

The results of the ADME study showed that all the compounds' log *P* values were found to be within limits (*i.e.* less than five). AlogP is a critical parameter that affects drug bioavailability,

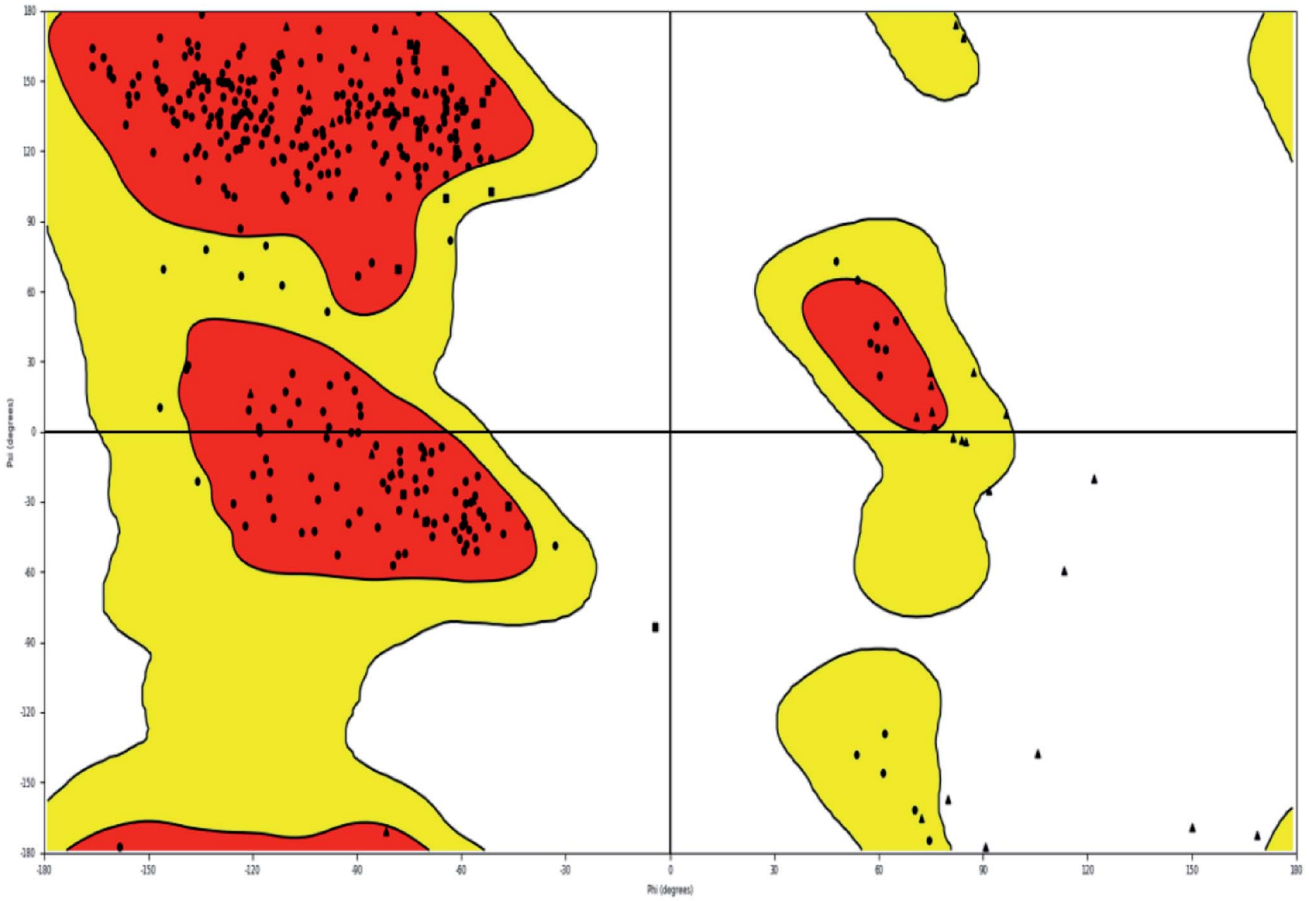

Fig. 3 Ramachandran plot of 1OKE.

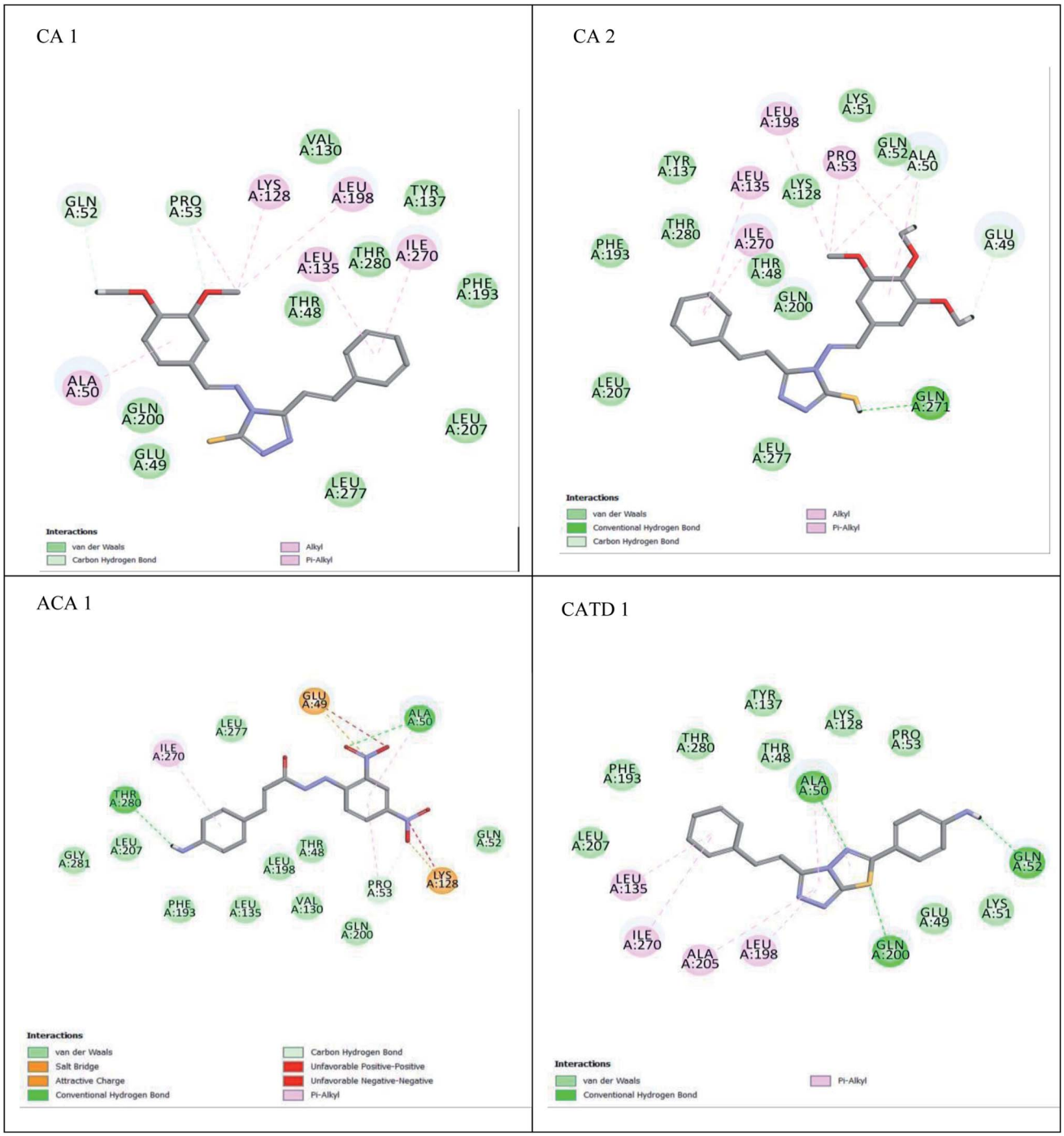

Fig. 4 2D interaction of the compounds.

membrane permeability and drug delivery and clearance paths. This parameter is also important in drug pharmacological and toxicological properties. Plasma protein binding is another parameter to assess the concentration of a medicinal compound. It may be restrictive or permissive and is known to affect drug distribution. A Bayesian score ≥2.226 was observed for the compounds, indicating their likelihood to bind to a carrier protein in the blood. All compounds had a >140 polar surface area (Table 3), indicating the potential for high intestinal absorption (Fig. 5). All of the compounds were found to have high blood barrier levels. All compounds were CYP2D6 non-inhibitors, with none associated with significant drug interaction toxicity.

The MM-GBSA approach for binding free energy calculation revealed that van der Waals and coulombic terms were the most relevant positive contributors. A preferential trend towards the van der Waals component was observed, as indicated by the van der Waals and Coulomb energy interactions between −17.19 and −57.5 kcal mol^{-1}, and −1.36 and −41.97 kcal mol^{-1},

Table 3 ADME properties of cinnamic acid analogues

Comp.	Solubility[a]	BBB[b]	CYP2D6[c]	Hepatoxicity[d]	PPB[e]	Absorption[f]	AlogP9[g]	PSA[h]
CA 1	2	1	FALSE	TRUE	TRUE	3	4.845	152.427
CA 2	2	1	FALSE	FALSE	TRUE	2	3.335	116.194
CA 3	2	1	FALSE	FALSE	TRUE	2	3.135	136.491
CA 4	2	1	FALSE	TRUE	TRUE	3	3.308	166.139
CA 5	2	1	FALSE	TRUE	TRUE	3	3.118	142.319
CA 6	2	1	FALSE	TRUE	TRUE	2	3.214	132.178
CA 7	3	1	FALSE	TRUE	TRUE	3	4.105	153.234
CA 8	2	1	FALSE	TRUE	TRUE	2	3.214	150.178
CA 9	3	1	FALSE	TRUE	TRUE	2	3.578	146.714
CA 10	2	1	FALSE	TRUE	TRUE	3	3.468	150.546
CA 11	2	1	FALSE	TRUE	TRUE	2	3.752	162.482
CA 12	3	1	FALSE	TRUE	TRUE	3	3.312	138.814
CA 13	2	1	FALSE	TRUE	TRUE	2	3.562	157.178
CA 14	2	1	FALSE	TRUE	TRUE	2	3.421	142.278
ACA 1	2	1	FALSE	TRUE	TRUE	3	3.308	126.139
ACA 2	2	1	FALSE	TRUE	TRUE	3	3.178	143.116
ACA 3	3	1	FALSE	TRUE	TRUE	3	3.751	148.142
ACA 4	2	1	FALSE	TRUE	TRUE	3	3.892	156.178
CATD 1	2	1	FALSE	TRUE	TRUE	3	2.932	143.911
CATD 2	1	1	FALSE	FALSE	TRUE	4	4.513	137.954
CATD 3	2	1	FALSE	FALSE	TRUE	3	4.113	147.954
CATD 4	4	1	FALSE	FALSE	TRUE	4	2.625	150.491
CATD 5	1	1	FALSE	FALSE	TRUE	4	4.357	157.954
FMCV	2	1	FALSE	TRUE	TRUE	3	2.549	150.055
P02	2	2	FALSE	TRUE	TRUE	3	4.951	150.89

[a] Solubility level – 0 extremely low; 1 no very low but possible; 2 yes low; 3 yes good; 4 yes optimal; 5 no too soluble. [b] BBB – blood-brain barrier level – 0 very high; 1 high; 2 medium; 3 low; 4 undefined. [c] CYP2D13 – cytochrome 450 inhibition. [d] Hepatotoxicity. [e] PPB – plasma-protein binding. [f] Absorption – 1 very poor, 2 poor; 3 medium; 4 good. [g] AlogP98 – partition coefficient of octanol/water system, [h] PSA – polar surface area.

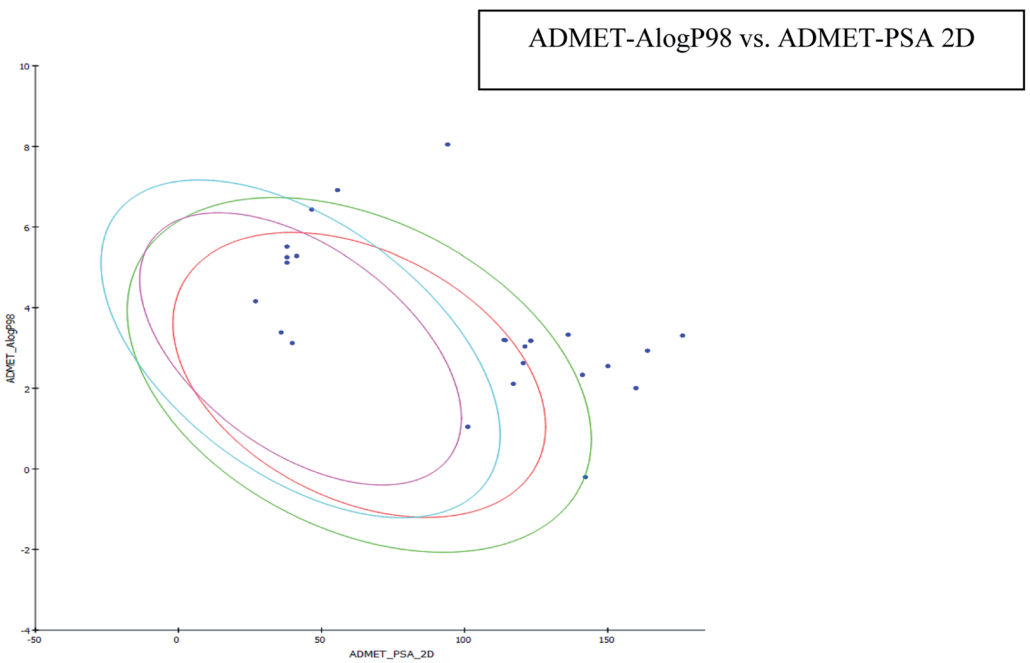

Fig. 5 Plot of PSA *versus* log *P* with 95% and 99% confidence limit ellipses.

respectively (Table 4). CA2 bounds best with DG (-75.87 kcal mol^{-1}), with a slightly higher van der Waals contribution (-43.1 kcal mol^{-1}), favourable lipophilic energy (25.67 kcal mol^{-1}), and a favourable coulomb energy term (-41.97 kcal mol^{-1}). van der Waals was deemed the driving force behind ligand binding.

Table 4 Binding free energy calculation using the prime/MM-GBSA approach

S. No.	Comp. code	ΔG bind (kcal mol^{-1})	ΔG Coulomb	ΔG vdW	ΔG H-bond	ΔG covalent	ΔG lipophilic
1	CA 1	−70.87	−41.97	−63.1	−6.46	10.44	−45.67
2	CA 2	−75.71	−64.22	−80.41	−2.14	−16.89	−61.27
3	CA 3	−69.31	23.56	−57.5	−2.5	−0.01	−46.19
4	CA 4	−68.22	−41.21	−63.24	−6.53	8.44	−38.42
5	CA 5	−51.47	−19.36	−75.55	−0.18	1.72	−37.68
6	CA 6	−51.3	−11.27	−69.4	−2.86	13.24	−30.19
7	CA 7	−62.49	−15.11	−47.19	−7.4	−8.27	−36.96
8	CA 8	−60.78	−21.56	−48.43	−5.69	14.76	−32.12
9	CA 9	−56.286	−23.041	−56.205	−3.13	15.602	−44.468
10	CA 10	−54.268	−21.465	−60.112	−1.684	11.377	−43.595
11	CA 11	−60.243	−46.524	−55.803	2.073	5.477	−35.024
12	CA 12	−58.177	−53.035	−73.522	1.433	11.726	−38.407
13	CA 13	−54.562	−12.145	−77.397	−0.208	24.994	−43.145
14	CA 14	−57.471	−21.185	−63.714	1.699	19.058	−36.654
15	ACA 1	−54.562	−11.145	−79.397	−0.208	24.994	−43.145
16	ACA 2	−57.471	−21.185	−63.714	1.699	19.058	−36.654
17	ACA 3	−57.177	−50.035	−73.522	1.433	11.726	−39.407
18	ACA 4	−51.043	61.524	−79.803	2.073	5.477	−51.024
19	CATD 1	−56.286	−23.041	−56.205	−3.13	15.602	−44.468
20	CATD 2	−54.268	−21.465	−60.112	−1.684	11.377	−43.595
21	CATD 3	−60.243	−46.524	−15.803	2.073	5.477	−35.024
22	CATD 4	−58.177	−53.035	−73.522	1.433	11.726	−38.407
23	CATD 5	−48.770	−55.237	−69.722	1.521	10.614	−40.701
24	Fmcv	−58.177	−40.015	−40.221	1.278	11.425	−29.728
25	PO2	−63.97	−23.19	−41.47	−4.47	−4.32	0000

3.2. *In silico* study of cinnamic acid analogues against FK506-binding protein (FKBP) from *Aedes aegypti* (PDB ID 3UQI)

In PyRx, binding affinity parameters were considered for selecting the best "HITS" and compared with the known Co-crystal. PyRx binding energy is the interaction energy between the protein and the ligand. This value strongly indicates the extent of the interaction of proteins and ligands. The synthesized molecules whose binding energy was above the co-crystal FKBP-type peptidyl-prolyl *cis–trans* isomerase (−4.7) are shown in Table 5, indicating that the compounds were effectively bound to the active site of 3UQI. The hydrogen bonds and Pi–Pi interactions of these compounds were analyzed. The CA 2 showed the highest binding affinity for 3UQI (−7.8) and the 3UQI-6 protein CA 2 complex made one conventional-hydrogen bonding (Arg 43), four hydrophobic interactions (Glu 55, Ile 57, Phe 100 and Trp 60), and two pi–alkyl interactions (Val 56, and Tyr 57).

3.3. Prediction of insecticide likeness

Insecticides are likely to have significantly different bioavailability related property profiles compared with drugs. Therefore, we evaluated the insecticide likeness of our cinnamic acid analogues by the radar (Fig. 6) (the pink area represents the optimal range for each property) and histograms at first glance or according to the insecticide likeness scores (the higher the score, the better the pesticide likeness of our compounds). Our compounds have shown properties which are similar to those of the standard insecticide flupyradifurone, which are given in Table 6.

3.4. Chemistry

Cinnamic acid derivatives were prepared as depicted in Schemes 1–3. The selected cinnamic acids were substituted using hydrazine hydrate at positions 2, 4, and 7 of the phenyl ring with a nitrogen linker. To increase the lipophilicity, permeability, and receptor binding affinity of the cinnamic acid scaffold, 4-amino cinnamic acid (ACA) was esterified using DCC/HOBT to get amino cinnamic acid ester (Scheme 1). The hydrazides were then subjected to conjugation with ACE to yield the cinnamic acid conjugates *viz.*, ACA-1, ACA-2, ACA-3, and ACA-4. Cinnamic acid triazole (**8**) was used to synthesize compounds *viz.*, CA-1, CA-2, CA-3, CA-4, CA-5, CA-6, CA-7, CA-8, CA-9, CA-10, CA-11, CA-12, CA-13, and CA-14 by Schiff reaction using the same reaction conditions (Scheme 2). The cinnamic acid thiadiazole derivatives *viz.*, CATD-1, CATD-2, CATD-3, CATD-4, and CATD-5 have been synthesized by reactions between the CAT and different benzoic acids (Scheme 3). All the conjugates were purified by column chromatography (ethyl acetate and *n*-hexane) and characterized by spectroscopic analysis like ^{1}H NMR, ^{13}C NMR, and mass spectra.

3.5. Biological studies

3.5.1. *In vitro* cytotoxicity assay. The MTT assay was performed to screen the synthesized compounds on Vero cells, and the results are shown in Table 7. Even at higher concentrations

Table 5 Binding energies of synthesized compounds against FK506-binding protein (FKBP) of *Aedes aegypti* (PDB ID 3UQI)

Ligand	Binding energy (kcal mol^{-1})	2D interactions
CA 2	−7.8	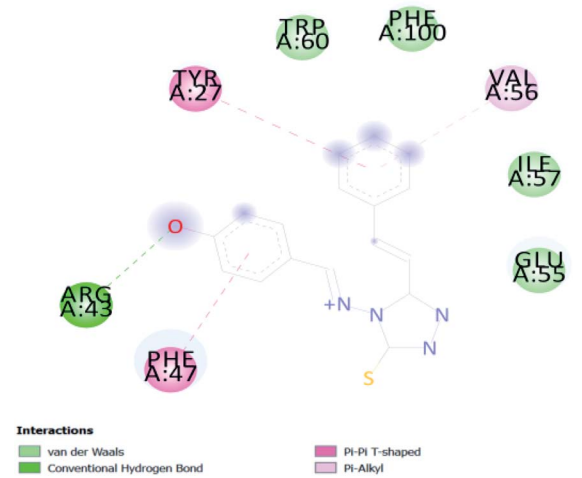
CATD 4	−7.3	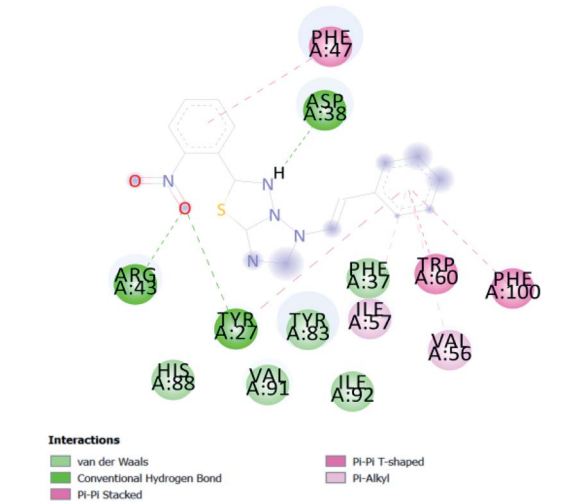
CATD 3	−7	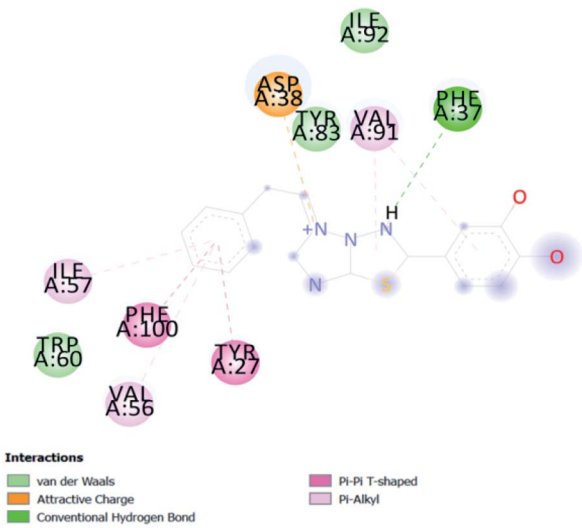

Table 5 (*Contd.*)

Ligand	Binding energy (kcal mol^{-1})	2D interactions
ACA 1	−6.9	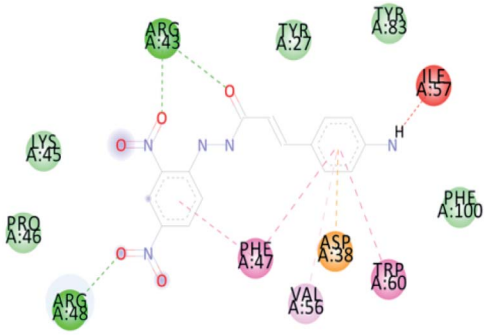
CA 4	−6.8	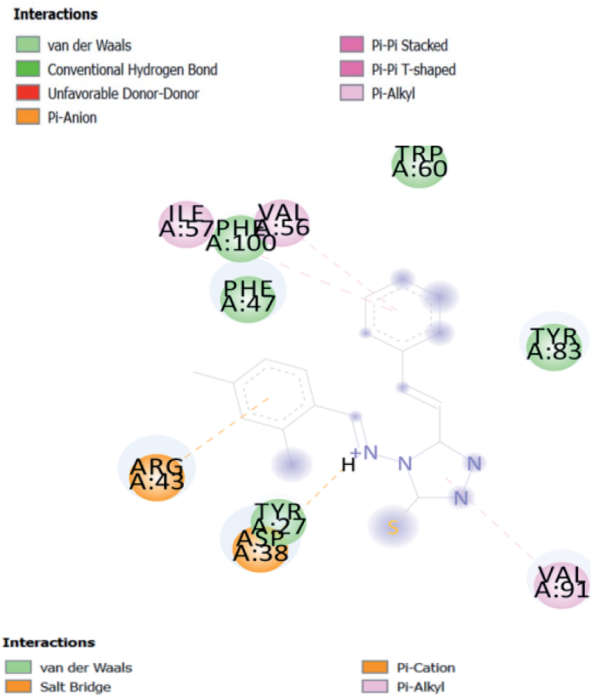
CA 14	−6.7	

Table 5 (*Contd.*)

Ligand	Binding energy (kcal mol^{-1})	2D interactions
CA 6	−6.5	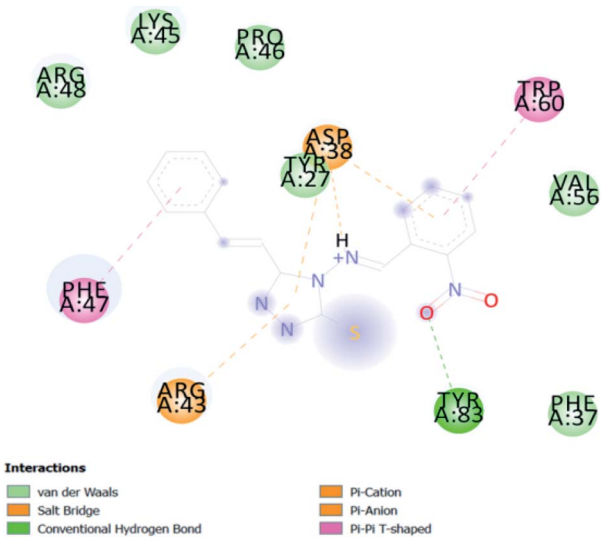
ACA 3	−6.5	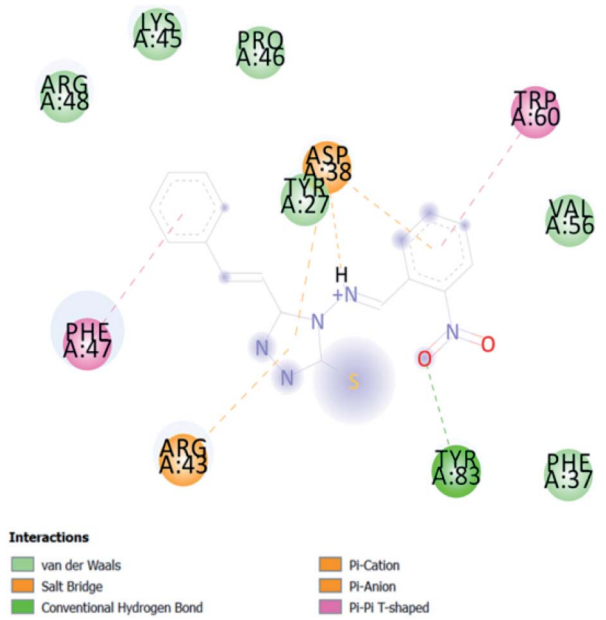

Table 5 (*Contd.*)

Ligand	Binding energy (kcal mol^{-1})	2D interactions
CA 14	−6.4	
Co-crystal	−4.7	

Table 5 (*Contd.*)

Ligand	Binding energy (kcal mol^{-1})	2D interactions

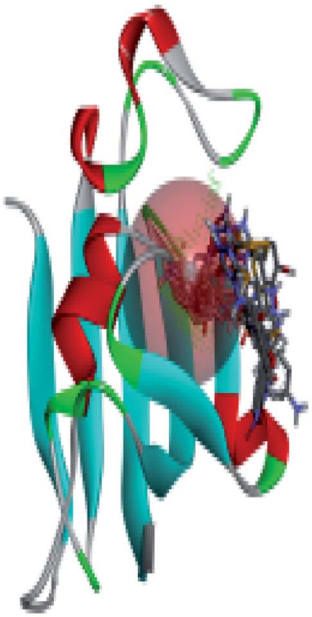

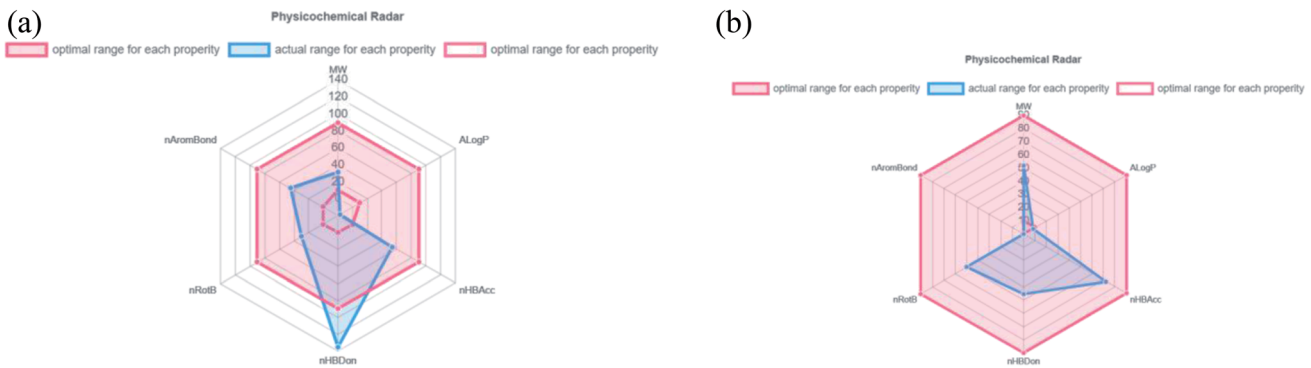

Fig. 6 Correlation plot (fitness graph between observed and predicted binding affinity for training): (a) ACA-2 and (b) standard flupyradifurone.

of cinnamic acid derivatives for treatment, no cytotoxicity was observed in normal cells.

3.5.2. Hemolytic assay. The hemolytic activities of synthesized compounds were tested at various concentrations (25, 50, and 100 μg ml^{-1}). The least hemolysis was 50 μg ml^{-1} (Table 8). Because compounds affect blood cells explicitly or implicitly, blood compatibility research is critical at the nanotoxicity level. Erythrocyte circulation through various organs leads to cell membrane injury, DNA damage, and congenital malformation. In this case, biocompatibility analyses of ligands that release erythrocytes were more critical than compound toxicity analyses.

3.5.3. Larvicidal activity. The larvae's growth (mortality) was analyzed for the selected compounds to understand the relationship between compound growth rate and larvae mortality. During the 72 h exposure period, the LC_{50} and LC_{90} for the best larvicidal activity were determined. Among all the compounds tested, CA 2 strains demonstrated significant larvicidal activity at minimum concentrations even after 24, 48, and 72 h of subjection (Table 11).

Different concentrations (50, 100, 150, 200 and 250 μg ml^{-1}) were used to determine the mortality after 24, 48 and 72 h of subjection. The mortality rate is affected by concentration and subjection period. However, observing CA 2 treatment at a minimum concentration for 24 and 48 hours resulted in the highest mortality range. ACA 4 showed slow mortality in the 24, 48, and 72 h exposure times, but they inhibited larval

Table 6 Insecticide likeness of cinnamic acid analogues[a]

S. No.	Compound code	MW (g mol^{-1})	AlogP	HBA	HBD	*n*RotB	*n*AromB	RDL	QEI	GAU
1	CA2	322.089	2.76	4	1	4	17	0.807	0.567	5.021
2	CA8	384.004	3.783	4	0	4	17	0.945	0.574	4.466
3	CA10	385.012	1.954	4	1	4	12	0.9	0.65	4.979
4	CA12	337.112	1.002	4	1	5	12	1.045	0.697	5.369
5	CA13	324.104	1.226	4	1	4	12	0.942	0.678	5.077
6	CA14	351.079	3.543	4	0	5	17	1.097	0.637	5.142
7	ACA4	359.027	1.475	4	3	4	13	0.818	0.483	6.023
8	ACA2	177.09	−0.858	3	3	3	7	1.326	0.284	4.417
9	CATD2	320.11	0.729	4	0	3	13	1.184	0.707	4.255
10	Flupyra difurone (standard)	289.056	0.418	4	1	5	0	1.368	0.714	5.913
11	Limits (as per)	60–500	0.52–4.5	0–5	0–2	0–9	0–14			

[a] MW: molecular weight, AlogP: lipophilicity, HBA: hydrogen bond acceptors, HBD: hydrogen bond donors, *n*RotB: number of rotatable bonds (flexibility), *n*AromB: number of aromatic bonds, RDL: relative drug likelihood, QED: quantitative estimate of drug-likeness, Gau.: gaussian scoring function.

Table 7 IC_{50} cytotoxicity studies

S. No.	Compound	Vero (IC_{50} μg ml^{-1})
1	Famciclovir	270 ± 0.20
2	Glabranin	252 ± 0.20
3	CA 1	309 ± 0.21
4	CA 2	321 ± 0.12
5	CA 3	314 ± 0.12
6	CA 4	210 ± 0.03
7	CA 5	223 ± 0.05
9	CA 6	312 ± 0.05
10	CA 7	295 ± 0.04
11	CA 8	318 ± 0.02
12	CA 9	235 ± 0.05
13	CA 10	241 ± 0.01
14	CA 11	229 ± 0.02
15	CA 12	252 ± 0.04
16	CA 13	238 ± 0.01
17	CA 14	240 ± 0.03
18	ACA 1	285 ± 0.05
19	ACA 2	242 ± 0.02
20	ACA 3	254 ± 0.03
21	ACA 4	328 ± 0.02
22	CATD 1	211 ± 0.01
23	CATD 2	218 ± 0.02
24	CATD 3	270 ± 0.20
25	CATD 4	252 ± 0.20
26	CATD 5	314 ± 0.21

Table 8 Hemolytic assay

Compound	Conc. (PPM)	Absorbance	Hemolytic (%)
FMVC	100	3.244	8.901
	50	3.065	6.448
	25	2.823	4.802
CATD-2	100	3.188	5.759
	50	3.033	5.367
	25	2.732	4.605
CA-2	100	2.208	3.278
	50	1.977	2.003
	25	1.783	1.202
CA-14	100	2.66	4.422
	50	2.62	4.326
	25	1.367	1.149
CA-13	100	3.121	5.589
	50	2.994	5.268
	25	2.623	4.329
ACA-4	100	3.228	3.460
	50	2.739	2.122
	25	2.389	1.736
CA-12	100	3.178	5.734
	50	3.037	5.377
	25	2.55	4.144
Glabranin	100	2.974	5.217
	50	2.775	4.713
	25	1.437	2.326
DMSO		0.851	0

development at the early pupal stage. At the cellular level, some damage may occur (Fig. 7 and Table 10)

3.5.4. Histopathological analysis. Midgut epithelial cell evaluations revealed the presence of flatter cells, with a translucent cytoplasm running through one-third of the midgut length in the anterior midgut. Apical swelling of varying degrees was observed into the gut lumen in simple cells, leading to reduced intercellular interactions with neighbouring cells and degeneration of nuclei and brush line, as observed in control larvae. The posterior midgut was characterized by epithelial cells, with the dark cells (in control parts) possessing stable intercellular connection around lateral plasma membranes, normal nuclei, and brush line, as well as a normal sticky basement membrane.

In both larvae, the drug samples CA 2, CA 14, ACA 4, and CATD 2 resulted in severe lesions that primarily affected the midgut epithelium and the caeca to a lesser extent (Fig. 8).

Table 9 Test set

S. No.	Compound code	Molecular formula	Predicted pLC_{50} (μM)
1	CA 5	$C_{20}H_{22}N_4O_3S$	6.8780
2	CA 9	$C_{17}H_{15}N_5O_2S$	6.7218
3	ACA 1	$C_{15}H_{13}N_5O_5$	6.6914
4	CATD 1	$C_{17}H_{15}N_5S$	6.8921
5	CATD 5	$C_{17}H_{13}ClN_4S$	6.8987

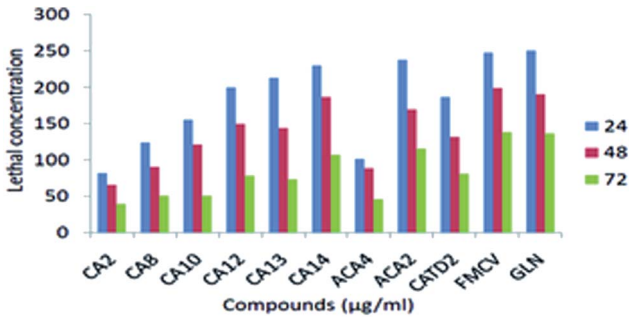

Fig. 7 Larvicidal activity of different synthesized compounds against *Aedes aegypti*.

Histopathological variations were observed qualitatively based on location along the midgut and quantitatively based on incubation time. After 72 h of infection, anterior midgut cells did not differ morphologically from normal ones, but for mild apical lysis of transparent cells and no lateral junctional complex disturbances. Compared with monitors, transparent cell lysis was accelerated at the brush border, basal membranes, and cytoplasmic organelles before bursting into the gut lumen. A posterior midgut partial lysis was initiated following local detachment in dark cells, with basal membrane dilatation and loss of the peritrophic membrane, with enlargement of cells.

3.6. QSAR studies

The QSAR approach is used to identify the structural parameters for the enhanced bioactivity, which leads to the design of the new scaffold with improved biological effects. A QSAR correlation between larvicidal activities with the series of nineteen synthesized compounds was performed by multiple linear regression analysis. The LC_{50} (μM) values of the training set were first converted into a negative logarithmic scale (pLC_{50}) to achieve the normal distribution (Table 9). The derived QSAR model shows a good correlation between biological activity and

Table 10 log probit analysis of the larvicidal activity of tested compounds using SPSS 10[a]

Sample	Time (h)	LC_{50} (ppm)	95% LCL to UCL (ppm)	LC_{90} (ppm)	95% LCL to UCL (ppm)	Intercept	Slope	χ^2 value
CA2	24	82.150	060.708–124.814	109.721	−2.821	0.013	0.379	0.944
	48	65.342	097.638–186.016	96.144	−1.496	0.010	0.269	0.966
	72	38.685	010.970–118.460	79.422	−1.014	0.012	0.694	0.875
CA8	24	123.885	054.531–167.921	265.404	−1.122	0.009	1.217	0.749
	48	90.793	048.979–118.498	165.954	−1.548	0.017	0.833	0.842
	72	50.137	013.314–090.657	122.039	−1.516	0.023	0.763	0.858
CA10	24	155.581	094.019–162.201	210.414	−2.643	0.014	0.802	0.849
	48	121.420	081.828–140.880	172.096	−1.396	0.011	0.357	0.949
	72	50.285	031.654–107.105	122.913	−1.129	0.015	0.901	0.825
CA12	24	200.037	167.480–258.244	295.409	−2.957	0.013	1.939	0.585
	48	149.114	126.982–224.856	229.123	−1.667	0.010	0.236	0.972
	72	78.125	054.652–130.490	166.552	−1.278	0.013	0.453	0.929
CA13	24	213.150	190.708–244.8 14	309.721	−2.829	0.013	0.379	0.944
	48	143.342	097.638–186.016	266.144	−1.496	0.010	0.269	0.966
	72	73.685	050.970–108.460	189.422	−1.014	0.012	0.694	0.875
CA14	24	230.111	215.757–615.686	389.073	−2.491	0.009	0.748	0.862
	48	186.546	175.129–259.690	280.065	−2.830	0.014	0.381	0.944
	72	106.898	084.119–180.863	237.905	−1.339	0.010	0.330	0.954
CA15	24	227.608	213.318–466.134	353.117	−2.858	0.011	1.463	0.691
	48	209.434	169.671–300.198	308.221	−2.084	0.010	1.144	0.766
	72	125.295	118.817–194.307	260.714	−1.888	0.012	0.409	0.938
ACA4	24	101.176	89.885–276.910	358.428	−2.636	0.011	1.446	0.695
	48	88.823	62.926–175.039	323.217	−2.103	0.010	1.723	0.632
	72	47.347	032.563–93.148	240.784	−1.702	0.012	1.755	0.625
ACA2	24	238.252	227.451–491.294	306.392	−4.857	0.019	0.628	0.890
	48	169.114	126.982–224.856	259.123	−1.667	0.010	0.236	0.972
	72	115.394	068.626–148.713	207.730	−1.445	0.013	1.177	0.759
CATD2	24	187.076	168.650–250.990	311.453	−1.928	0.010	0.483	0.923
	48	131.513	098.030–168.174	241.010	−1.539	0.012	1.823	0.610
	72	086.556	068.446–108.142	179.532	−1.193	0.014	2.145	0.543
FMCV	24	247.578	188.650–280.990	311.453	−1.928	0.010	0.483	0.723
	48	202.983	168.030–230.174	241.010	−1.293	0.022	1.823	0.501
	72	138.785	118.446–188.142	179.532	−1.193	0.016	2.145	0.443
GLA	24	258.231	230.650–290.990	311.453	−1.782	0.014	0.538	0.823
	48	198.960	172.030–268.174	241.010	−1.539	0.017	1.675	0.610
	72	140.249	1298.446–180.142	179.532	−1.132	0.011	2.238	0.534

[a] LCL: lethal concentration limit, UCL: upper concentration limit, LC_{50}: lethal concentration 50%, LC_{90}: lethal concentration 90%, estimated air concentration of a substance administered *via* inhalation route, and DF: degree of freedom.

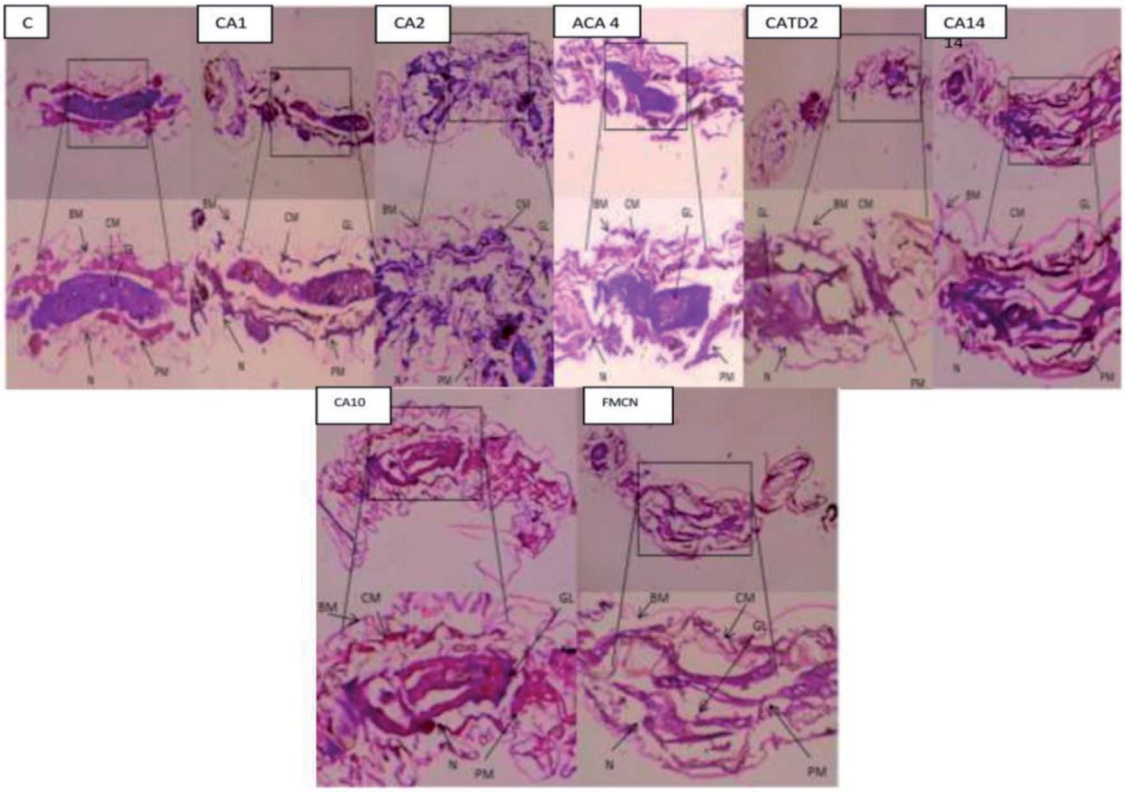

Fig. 8 Histopathological observation of 72 h of exposure to selected compounds CA2, CA14, ACA4, and CATD 2 against *A. aegypti*. The black-coloured arrow refers to damage in mosquitoes: B.M. – basal membrane; N – nucleus border; GL – gut lumen; PM – peritrophic membrane; CM – cytoplasmic membrane of the larvae compared to the control.

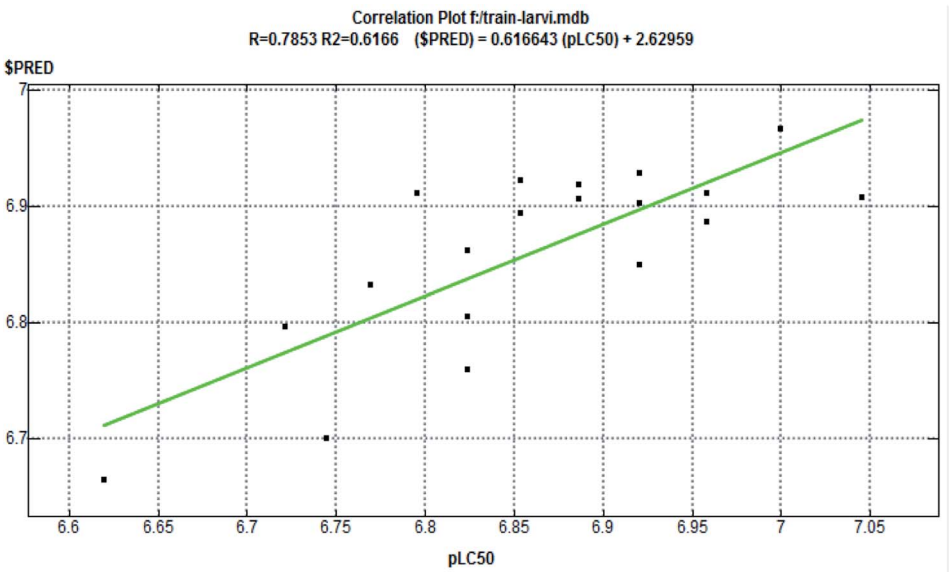

Fig. 9 Correlation plot (fitness graph between observed and predicted binding affinity for training).

parameters, further validated through test set compounds (Table 11). The descriptors showed a positive correlation among all parameters selected for the QSAR model. The positive coefficients suggest that including such hybrid structures together leads to an increase in biological activity. Further, the regression graph was plotted for pLC_{50} *vs.* $PRED. (Fig. 9). The cross-validated correlation coefficient (r^2) value is 0.61664, and the root mean square error value is 0.06233.

Table 11 Compounds with the observed and predicted activity of C.A. derivatives used in the training set

S. No.	Comp. code	LC50 (μM)	pLC_{50} (μM)		
			Observed	Predicted	Residual
1	CA 1	0.13	6.8861	6.9184	−0.0323
2	CA 2	0.09	7.0458	6.9070	0.1388
3	CA 3	0.12	6.9208	6.9290	−0.0082
4	CA 4	0.16	6.7959	6.9113	−0.1154
5	CA 6	0.14	6.8539	6.8945	−0.0406
6	CA 7	0.11	6.9586	6.8864	0.0722
7	CA 8	0.15	6.8239	6.8617	−0.0378
8	CA 10	0.14	6.8539	6.9230	−0.0691
9	CA 11	0.17	6.7696	6.8326	−0.0630
10	CA 12	0.11	6.9586	6.9119	0.0467
11	CA 13	0.12	6.9208	6.9025	0.0183
12	CA 14	0.18	6.7447	6.7000	0.0447
13	ACA 2	0.15	6.8239	6.8050	0.0189
14	ACA 3	0.19	6.7212	6.7963	−0.0751
15	ACA 4	0.10	7.0000	6.9670	0.0330
16	CATD 2	0.13	6.8861	6.9068	−0.0207
17	CATD 3	0.12	6.9208	6.8501	0.0707
18	CATD 4	0.15	6.8239	6.7601	0.0638
19	FMCV	0.24	6.6198	6.6645	−0.0447

The formula for the generated QSAR linear model is

$$pLC_{50} = 8.45519 - 0.02346 \times AM1\_dipole - 0.00034 \times TPSA + 0.00052 \times E\_vdw + 0.08078 \times AM1\_LUMO + 0.16393 \times AM1\_HOMO - 0.01678 \times mr + 0.01392 \times \log P(o/w)$$

Thus, the developed QSAR model can be applied to develop potent modified molecules with nitrogen, sulfur, and oxygen atoms, as potential anti-dengue agents.

4. Conclusion

The present research study suggests that our synthesized compounds may be the "LEAD" molecules for early DENV inhibition, which prevents or lessens the chances of patients progressing to dengue hemorrhagic fever/dengue shock syndrome. Cost-effectiveness is a crucial issue for this still poverty-linked disease, and this issue is also figured out by selecting early DENV inhibitors. Overall, this study concludes CA-2 and ACA-4 as potent compounds for biologically controlling *Aedes aegypti*. The docking studies also support the insecticidal potency of the synthesized compounds. Interestingly, *in silico* docking findings show that the molecule CA-2 also regulates the 1OKE protein through the β-OG bag. As a result, CA-2 may be used as a lead molecule in anti-viral entry inhibition. The QSAR model developed may be used to design candidates, with nitrogen, sulfur, and oxygen atom substituents, as promising anti-dengue compounds. The compounds CA 2 and ACA 4 may also be considered lead compounds for other mosquito-borne viral diseases.

Funding

The work was supported through the JSS Academy of Higher Education & Research, Mysuru, to provide a research grant for the study (ref. no. REG/DIR(R)/URG/54/2011–12/10887/1, Date: 23.02.2017).

Conflicts of interest

The authors declare that there are no conflicts of interest.

References

1 S. P. Lim, Q. Y. Wang, C. G. Noble, Y. L. Chen, H. Dong, B. Zou, F. Yokokawa, S. Nilar, P. Smith, D. Beer and J. Lescar, *Antiviral Res.*, 2013, **100**, 500.
2 C. G. Noble, Y. L. Chen, H. Dong, F. Gu, S. P. Lim, W. Schul, Q. Y. Wang and P. Y. Shi, *Antiviral Res.*, 2010, **85**, 450.
3 D. J. Gubler, *Trends Microbiol.*, 2002, **10**, 100.
4 S. S. Whitehead, J. E. Blaney, A. P. Durbin and B. R. Murphy, *Nat. Rev. Microbiol.*, 2007, **5**, 518.
5 R. Fritz, K. Stiasny and F. X. Heinz, *J. Cell Biol.*, 2008, **183**, 353.
6 Y. Modis, S. A. Ogata, D. E. Clements and S. C. Harrison, *Nature*, 2004, **427**, 313.
7 K. Stiasny, C. Kossl, J. Lepault, F. A. Rey and F. X. Heinz, *PLoS Pathog.*, 2007, **3**, 20.
8 T. Kampmann, D. S. Mueller, A. E. Mark, P. R. Young and B. Kobe, *Structure*, 2006, **14**, 1481.
9 Z. Zhou, M. Khaliq, J. E. Suk, C. Patkar, L. Li, R. J. Kuhn and C. B. Post, *ACS Chem. Biol.*, 2008, **19**, 765.
10 Q. Y. Wang, S. J. Patel, E. Vangrevelinghe, H. Y. Xu, R. Rao, D. Jaber, W. Schul, F. Gu, O. Heudi, N. L. Ma, M. K. Poh, W. Y. Phong, T. H. Keller, E. Jacoby and S. G. Vasudevan, *Antimicrob. Agents Chemother.*, 2009, **53**, 1823.
11 Y. Qian, H. J. Zhang, H. Zhang, C. Xu, J. Zhao and H. L. Zhu, *Bioorg. Med. Chem.*, 2010, **18**, 4991.
12 C. R. Rees, J. M. Costin, R. C. Fink, M. McMichael, K. A. Fontaine, S. Isern and S. F. Michael, *Antiviral Res.*, 2008, **80**, 135.
13 R. Yin, Z. Ding, X. Liu, L. Mu, Y. Cong and T. Stoeger, *J. Virol. Methods*, 2010, **167**, 107.
14 D. R. Green and F. Llambi, *Cold Spring Harbor Perspect. Biol.*, 2015, **7**, a006080.
15 G. S. Singh, *Eur. J. Med. Chem.*, 2009, **44**, 2265.
16 B. Podobnik, J. Stojan, L. Lah, N. Krasevec, M. Seliskar, T. L. Rizner, D. Rozman and R. Komel, *J. Med. Chem.*, 2008, **51**, 3480.
17 R. R. Craig, M. C. Joshua, C. F. Ryan, M. M. Matthew, A. F. Krystal, I. Sharon and F. M. Scott, *Antiviral Res.*, 2008, **80**, 135.
18 F. M. Scott, I. Sharon and M. C. Joshua, *US Pat.*, US2011/010037/A1, 2011.

19 C. D. Andersson, B. Y. Chen and A. Linusson, *Proteins*, 2011, **79**, 1363.
20 K. R. Cousins, Chem draw ultra 12.0, *J. Am. Chem. Soc.*, 2011, **133**, 8388.
21 T. Usha, K. G. Arvind, L. Syed, H. P. Prashanth, T. Madhan Mohan, P. Veena and K. M. Sushil, *Asian Pac. J. Cancer Prev.*, 2015, **15**, 10345.
22 T. Usha, S. K. Middha and A. K. Goyal, *J. Biomed. Res.*, 2014, **28**, 406.
23 V. B. Sulimov, D. C. Kutov and A. V. Sulimov, *Curr. Med. Chem.*, 2019, **26**, 7555.
24 K. Kalani, J. Agarwal, S. Alam, F. Khan, A. Pal and S. K. Srivastava, *PLoS One*, 2013, **8**, e74761.
25 S. Sarvagalla, V. K. Singh, Y. Y. Ke, H. Y. Shiao, W. H. Lin, H. P. Hsieh, H. Hsu and M. S. Coumar, *J. Comput.-Aided Mol. Des.*, 2015, **29**, 89.
26 T. Geerts and Y. Vander Heyden, *Comb. Chem. High Throughput Screening*, 2011, **14**, 339.
27 M. Kurokawa, A. Wadhwani, H. Kai, M. Hidaka, H. Yoshida, C. Sugita, W. Watanabe, K. Matsuno and A. Hagiwara, *Phytother. Res.*, 2016, **30**, 797.
28 R. Gopalan, M. Nanthagopal, S. Mahalingam, G. K. Arumugam, S. K. Samuthirarajan, M. Narayanasamy and I. Sakkanan Ilango, *Nano Express*, 2021, **2**, 010010.
29 R. G. Monnerat, A. C. Batista, P. T. de Medeiros, E. S. Martins, V. M. Melatti, L. B. Praça, V. F. Dumas, C. Morinaga, C. Demo and A. C. M. Gomes, *Biol. Control*, 2007, **41**, 291.
30 B. Banumathi, T. Vaseeharan, S. Chinnasamy, M. Vijayakumar, N. S. Govindarajan, P. Vijayan, U. Muthukumaran and G. Benelli, *J. Cluster Sci.*, 2017, **28**, 2857.
31 T. Prabha and T. Sivakumar, *Asian J. Pharm. Clin. Res.*, 2018, **11**, 233.
32 S. M. Hipparagi and M. D. Bhanushali, *J. Sci. Soc.*, 2013, **40**, 80.
33 Molecular Operating Environment (MOE): Chemical Computing Group Inc. 2009; 1010 Sherbooke St. West, Suite #910, Montreal, QC, Canada, H3A 2R7.
34 L. K. Wolf, *Chem. Eng. News*, 2009, **87**(45), 48.
35 Y. C. Chen, *Trends Pharmacol. Sci.*, 2015, **36**(2), 78–95.